Supporting Information

Imide-Based Multi-Electron Anolytes as High-Performance Materials in Nonaqueous Redox Flow Batteries

Nicolas Daub,[1] René A. J. Janssen,[1,2]* and Koen H. Hendriks[1,2]*

[1] Molecular Materials and Nanosystems & Institute for Complex Molecular Systems, Eindhoven University of Technology, 5600 MB Eindhoven, The Netherlands, E-mail: r.a.j.janssen@tue.nl

[2] Dutch Institute for Fundamental Energy Research, De Zaale 20, 5612 AJ Eindhoven, The Netherlands, E-mail: k.h.hendriks@differ.nl

Experimental

General Information

All commercial chemicals were used as received unless stated otherwise. All reactions were performed under nitrogen atmosphere unless stated otherwise. NMR spectra were obtained on a Bruker 400 MHz spectrometer. ^{1}H and ^{13}C chemical shifts are reported in parts per million (ppm) relative to TMS, with the residual solvent peak used as an internal reference. For matrix assisted laser desorption ionization time of flight (MALDI-TOF) mass spectrometry a Bruker Autoflex Speed spectrometer was used. Microwave reactions were performed on a Biotage Initiator+.

Synthesis of used compounds

General Procedure A: Synthesis of the phthalimide compounds with lower solubility (1a, 1b, 1e): A 5 mL microwave tube was loaded with phthalic anhydride (1.35 mmol, 1.0 eq) and sealed. It was then gently heated under vacuum and refilled with argon. This was repeated 3 times. Afterwards, acetic acid (1.78 mL) and the corresponding amine (1.49 mmol, 1.1 eq) were injected through the septum in the cap. The tube was heated for 10 minutes to 200 °C in a microwave reactor. After cooling down, the product crashed out and was filtered and washed with cold

methanol. If required, the crude product can be further purified by recrystallization from ethanol/ethyl acetate.

General Procedure B: Synthesis of the phthalimide compounds with higher solubility (1c, 1d, 1f, 1g): A 5 mL microwave tube was loaded with phthalic anhydride (1.35 mmol, 1.0 eq) and sealed. It was then gently heated under vacuum and refilled with argon. This was repeated 3 times. Afterwards, acetic acid (1.78 mL) and the corresponding amine (1.49 mmol, 1.1 eq) were injected through the septum in the cap. The tube was heated for 10 minutes to 200 °C in a microwave reactor. The mixture was poured into saturated sodium carbonate and extracted with DCM/MeCN (5/1). The organic phase was washed again with sodium carbonate and demi water and dried over $MgSO_4$ and concentrated.

General Procedure C: Synthesis of large quantities of the phthalimide compounds (1c, 1f): A nitrogen filled 250 mL Schlenk flask was loaded with phthalic anhydride (5.7 g, 38.48 mmol, 1.0 eq). It was then gently heated under vacuum and refilled with nitrogen. This was repeated 3 times. Afterwards, acetic acid (77 mL) and the corresponding amine (42.33 mmol, 1.1 eq) were injected. The flask was heated for 3 days to 120 °C. After cooling down, the mixture was neutralized with sodium bicarbonate and extracted with DCM/MeCN (5/1). The organic phase was washed again with sodium carbonate and demi water and dried over $MgSO_4$ and concentrated.

General Procedure D: Synthesis of pyromellitic diimide compounds with lower solubility (2a, 2b, 2d, 2e, 2f): A 5 mL microwave tube was loaded with pyromellitic dianhydride (2.29 mmol, 1.0 eq) and sealed. It was then gently heated under vacuum and refilled with argon. This was repeated 3 times. Afterwards, acetic acid (3.00 mL) and the corresponding amine (5.04 mmol, 2.2 eq) were injected through the septum in the cap. The tube was heated for 10 minutes to 200 °C in a microwave reactor. After cooling down, the product crashed out and was filtered and washed with cold methanol. If required, the crude product can be further purified by recrystallization from ethanol/ethyl acetate.

General Procedure E: Synthesis of pyromellitic diimide compounds with higher solubility (2c, 2g, 2h, 2i): A 5 mL microwave tube was loaded with pyromellitic dianhydride (2.29 mmol,

1.0 eq) and sealed. It was then gently heated under vacuum and refilled with argon. This was repeated 3 times. Afterwards, acetic acid (3.00 mL) and the corresponding amine (5.04 mmol, 2.2 eq) were injected through the septum in the cap. The tube was heated for 10 minutes to 200 °C in a microwave reactor. The mixture was poured into saturated sodium carbonate and extracted with DCM/MeCN (5/1). The organic phase was washed again with sodium carbonate and demi water and dried over $MgSO_4$ and concentrated.

General Procedure F: Synthesis of pyromellitic triimide compounds with lower solubility (3b, 3e): A 5 mL microwave tube was loaded with mellitic acid (1.46 mmol, 1.0 eq) and sealed in a nitrogen filled glovebox. Acetic acid (1.92 mL) and the corresponding amine (4.82 mmol, 3.3 eq) were injected through the septum in the cap. The tube was heated for 15 minutes to 200 °C in a microwave reactor. After cooling down, the product crashed out and was filtered and washed with cold methanol. If required, the crude product can be further purified by recrystallization from ethanol/ethyl acetate.

General Procedure G: Synthesis of pyromellitic triimide compounds with higher solubility (3c, 3d, 3f, 3g, 3h): A 5 mL microwave tube was loaded with mellitic acid (1.46 mmol, 1.0 eq) and sealed in a nitrogen filled glovebox. Acetic acid (1.92 mL) and the corresponding amine (4.82 mmol, 3.3 eq) were injected through the septum in the cap. The tube was heated for 15 minutes to 200 °C in a microwave reactor. The mixture was poured into saturated sodium carbonate and extracted with DCM/MeCN (5/1). The organic phase was washed again with sodium carbonate and demi water and dried over $MgSO_4$ and concentrated.

Synthesis of **1a:** Prepared by General Procedure A using methylamine to yield white crystals (481 mg, 88% yield). ^{1}H NMR (400 MHz, Chloroform-*d*) δ 7.87 – 7.82 (m, 2H), 7.74 – 7.68 (m, 2H), 3.19 (s, 3H).^{13}C NMR (100 MHz, Chloroform-*d*) δ 168.48, 133.86, 132.24, 123.17, 23.94. ^{1}H and ^{13}C NMR spectra are in agreement with literature.[1]

Synthesis of **1b:** Prepared by General Procedure A using isopropylamine to yield white crystals (590 mg, 85% yield). ^{1}H NMR (400 MHz, Chloroform-*d*) δ 7.83 – 7.80 (m, 2H), 7.71 – 7.68 (m, 2H), 4.54 (septet, J = 7.0 Hz, 1H), 1.50 (d, J = 7.0 Hz, 6H). ^{13}C NMR (100 MHz, Chloroform-*d*)

δ 168.38, 133.74, 132.13, 122.97, 43.00, 20.12. ^{1}H and ^{13}C NMR spectra are in agreement with literature.[1]

Synthesis of **1c:** Prepared by General Procedure B using 2-pentylamine to yield a yellowish oil (652 mg, 89% yield). For a larger quantity procedure C was employed using 2-pentylamine to yield a yellowish oil (7.19g, 86% yield).^{1}H NMR (400 MHz, Chloroform-*d*) δ 7.83 – 7.79 (m, 2H), 7.72 – 7.67 (m, 2H), 4.41 – 4.32 (m, 1H), 2.11 – 2.01 (m, 1H), 1.74 – 1.65 (m, 1H), 1.46 (d, J = 5.4 Hz, 3H), 1.35 – 1.21 (m, 2H), 0.90 (t, J = 5.4 Hz, 3H). ^{13}C NMR (100 MHz, Chloroform-*d*) δ 168.57, 133.75, 132.01, 123.00, 47.16, 35.81, 19.96, 18.69, 13.68. MS (MALDI) *m/z* calculated for $C_{13}H_{15}NO_2$(M): 217.1103, found 217.19.

Synthesis of **1d:** Prepared by General Procedure B using 2-ethyl-1-hexylamine to yield a colorless oil (650 mg, 74% yield). ^{1}H NMR (400 MHz, Chloroform-*d*) δ 7.87 – 7.82 (m, 2H), 7.74 – 7.68 (m, 2H), 3.53 (d, J = 7.2 Hz, 2H) 1.80 (septet, J = 6.2 Hz, 1H), 1.34 – 1.20 (m, 8H), 0.90 – 0.81 (m, 6H).^{13}C NMR (100 MHz, Chloroform-*d*) δ 168.30, 133.89, 132.11, 123.25, 69.40, 58.62, 37.30. ^{1}H and ^{13}C NMR spectra are in agreement with literature.[2]

Synthesis of **1e:** Prepared by General Procedure A using 2-methoxyethylamine to yield white crystals (557 mg, 87% yield). ^{1}H NMR (400 MHz, Chloroform-*d*) δ 7.87 – 7.82 (m, 2H), 7.74 – 7.68 (m, 2H), 3.90 (t, J = 5.7 Hz, 2H) 3.64 (t, J = 5.7 Hz, 2H), 3.35 (s, 3H). ^{13}C NMR (100 MHz, Chloroform-*d*) δ 168.58, 133.71, 132.00, 123.01, 41.77, 38.21, 30.42, 28.40, 23.74, 22.88, 13.94, 10.31. ^{1}H and ^{13}C NMR spectra are in agreement with literature.[3]

Synthesis of **1f:** Prepared by General Procedure B using 2-(2-methoxyethoxy)ethylamine to yield slightly yellowish crystals (740 mg, 88% yield). Prepared by General Procedure C using 2-(2-methoxyethoxy)ethylamine to yield slightly yellowish (8.83 g, 86% yield). ^{1}H NMR (400 MHz, Chloroform-*d*) δ 7.87 – 7.82 (m, 2H), 7.74 – 7.68 (m, 2H), 3.91 (t, J = 5.9 Hz, 2H) 3.75 (t, J = 5.9 Hz, 2H), 3.66 – 3.62 (m, 2H), 3.52 – 3.48 (m, 2H), 3.31 (s, 3H). ^{13}C NMR (100 MHz, Chloroform-*d*) δ 168.27, 133.89, 132.17, 123.22, 71.89, 69.91, 67.95, 59.01, 37.17. ^{1}H and ^{13}C NMR spectra are in agreement with literature.[4]

Synthesis of **1g:** Prepared by General Procedure B using 2-(2-methoxyethoxy)ethylamine to yield a yellowish oil (782 mg, 79% yield). ^{1}H NMR (400 MHz, Chloroform-*d*) δ 7.87 – 7.82 (m, 2H), 7.74 – 7.68 (m, 2H), 3.90 (t, J = 5.8 Hz, 2H) 3.74 (t, J = 5.9 Hz, 2H), 3.67 – 3.63 (m, 2H), 3.62 – 3.56 (m, 4H), 3.49 – 3.45 (m, 2H), 3.33 (s, 3H).^{13}C NMR (100 MHz, Chloroform-*d*) δ 168.24, 133.88, 132.14, 123.20, 71.86, 70.55, 70.53, 70.11, 67.90, 58.98, 37.27. ^{1}H and ^{13}C NMR spectra are in agreement with literature.[5]

Synthesis of **2a:** Prepared by General Procedure D using 33% methylamine in ethanol to yield white crystals (470 mg, 71% yield). ^{1}H NMR (400 MHz, Chloroform-*d*) δ 8.28 (s, 2H), 3.25 (s, H). ^{13}C NMR (100 MHz, Chloroform-*d*) δ 166.26, 137.32, 118.14, 24.52. ^{1}H and ^{13}C NMR spectra are in agreement with literature.[6]

Synthesis of **2b:** Prepared by General Procedure D using isopropylamine to yield white crystals (585 mg, 85% yield). ^{1}H NMR (400 MHz, Chloroform-*d*) δ 8.21 (s, 2H), 4.48 (q, J = 7.0 Hz, 2H), 1.52 (d, J = 7.0 Hz, 12H). ^{13}C NMR (100 MHz, Chloroform-*d*) δ 166.24, 137.11, 117.85, 43.91, 20.06. MS (MALDI) *m/z* calculated for$C_{16}H_{16}N_2O_4M^{\bullet-}$: 300.1116, found 300.18.

Synthesis of **2c:** Prepared by General Procedure E using 2-pentylamine to yield white crystals (431 mg, 88% yield). ^{1}H NMR (400 MHz, Chloroform-*d*) δ 8.21 (s, 2H), 4.45 – 4.36 (m, 2H), 2.10 – 2.00 (m, 2H), 1.77 – 1.68 (m, 2H), 1.49 (d, J = 6.9 Hz, 6H), 1.34 – 1.19(m, 4H), 0.91 (t, J = 7.4 Hz, 3H). ^{13}C NMR (100 MHz, Chloroform-*d*) δ 166.43, 137.00, 117.91, 48.03, 35.67, 19.94, 18.58, 13.62. MS (MALDI) *m/z* calculated for $C_{20}H_{24}N_2O_4M^{\bullet-}$: 356.1742, found 356.24.

Synthesis of **2d:** Prepared by General Procedure D using 2-ethyl-1-hexylamine to yield white crystals (878 mg, 87% yield). ^{1}H NMR (400 MHz, Chloroform-*d*) δ 8.26 (s, 2H), 3.64(d, J = 7.2 Hz, 4H), 1.85 (septet, J = 6.2 Hz, 2H), 1.39 – 1.21 (m, 16H), 0.95 – 0.85 (m, 12H).^{13}C NMR (100 MHz, Chloroform-*d*) δ 166.59, 137.16, 118.13, 42.53, 38.27, 30.50, 28.44, 23.86, 22.95, 14.02, 10.38. ^{1}H and ^{13}C NMR spectra are in agreement with literature.[7]

Synthesis of **2e:** Prepared by General Procedure D using 2-methoxyethylamine to yield white crystals (655 mg, 86% yield). ^{1}H NMR (400 MHz, Chloroform-*d*) δ 8.28 (s, 2H), 3.96 (t, J = 5.4

Hz, 4H), 3.66 (t, J = 5.5 Hz, 4H), 3.35 (s, 6H). ^{13}C NMR (100 MHz, Chloroform-*d*) δ 166.17, 137.23, 118.34, 69.07, 58.69, 38.02.

Synthesis of **2f:** Prepared by General Procedure D using 2-(2-methoxyethoxy)ethylamine to yield white crystals (429 mg, 89% yield). ^{1}H NMR (400 MHz, Chloroform-*d*) δ 8.27 (s, 2H), 3.96 (t, J = 5.6 Hz, 4H), 3.78 (t, J = 5.7 Hz, 4H), 3.66 – 3.62 (m, 4H), 3.51 – 3.46 (m, 4H), 3.30 (s, 6H). ^{13}C NMR (100 MHz, Chloroform-*d*) δ 166.14, 137.24, 118.19, 71.87, 69.92, 67.65, 59.01, 37.85. MS (MALDI) *m/z* calculated for $C_{20}H_{24}N_2NaO_8(M+Na)^+$: 443.1425, found 443.18.

Synthesis of **2g:** Prepared by General Procedure D using 2-(2-(2-methoxyethoxy)ethoxy)ethylamine to yield a grey gel (387 mg, 83% yield). The synthesis of large quantities of **2g** was performed as follows: A nitrogen filled 250 mL Schlenk flask was loaded with pyromellitic dianhydride (45.85 mmol, 1.0 eq). It was then gently heated under vacuum and refilled with nitrogen. This was repeated 3 times. Afterwards, acetic acid (91.7mL) and 2-(2-(2-methoxyethoxy)ethoxy)ethylamine (96.28 mmol, 2.1 eq) were injected under counter stream. The flask was heated for 3 days to 120 °C. After cooling down, the mixture was neutralized with sodium bicarbonate and extracted with DCM/MeCN (5/1). The organic phase was washed again with sodium carbonate and demi water and dried over $MgSO_4$ and concentrated. The resulting grey gel was re-dissolved in ethyl acetate and precipitated in hexane, filtered and washed with hexane. This was repeated three times to yield a grey powder (15.87 g, 68%).^{1}H NMR (400 MHz, Chloroform-*d*) δ 8.26 (s, 2H), 3.95 (t, J = 5.6 Hz, 4H), 3.77 (t, J = 5.7 Hz, 4H), 3.67 – 3.63 (m, 4H), 3.61 – 3.56 (m, 8H), 3.50 – 3.46 (m, 4H), 3.34 (s, 6H). ^{13}C NMR (100 MHz, Chloroform-*d*) δ 166.10, 137.22, 118.18, 71.86, 70.57, 70.53, 70.06, 67.62, 59.00, 37.93. MS (MALDI) *m/z* calculated for $C_{24}H_{32}N_2NaO_{10}(M+Na)^+$: 531.1949, found 531.23.

Synthesis of **2h:** Prepared by General Procedure E using 2-(2-(2-(2-methoxyethoxy)ethoxy)ethoxy)ethylamine to yield a brownish gel (605 mg, 89% yield). ^{1}H NMR (400 MHz, Chloroform-*d*) δ 8.26 (s, 2H), 3.95 (t, J = 5.5 Hz, 4H), 3.77 (t, J = 5.6 Hz, 4H), 3.67 – 3.58 (m, 20H), 3.54 – 3.51 (m, 4H), 3.36 (s, 6H). ^{13}C NMR (100 MHz, Chloroform-*d*) δ 166.10, 137.22, 118.20, 71.91, 70.57, 70.56, 70.55, 70.49, 70.03, 67.62, 59.01, 37.92. MS (MALDI) *m/z* calculated for $C_{28}H_{40}N_2NaO_{12}(M+Na)^+$: 610.2473, found 610.30.

Synthesis of **2i:** A 5 mL microwave tube was loaded with pyromellitic dianhydride (2.29 mmol, 1.0 eq) and sealed. It was then gently heated under vacuum and refilled with argon. This was repeated 3 times. Afterwards, acetic acid (3.00 mL) and 2-(2-(2-methoxyethoxy)ethoxy)ethylamine (2.29 mmol, 1.0 eq) were injected through the septum in the cap. The tube was heated for 5 minutes to 200 °C in a microwave reactor. Then, 2-pentylamine (2.29 mmol, 1.0 eq) were injected and heated again for 5 minutes to 200 °C in a microwave reactor. The mixture was poured into saturated sodium carbonate and extracted with DCM/MeCN (5/1). The organic phase was washed again with sodium carbonate and demi water and dried over $MgSO_4$ and concentrated. The residue was purified by column chromatography (silica gel, ethyl acetate/hexane 1/1) to yield a white gel, which solidifies after placing in the fridge (446 mg, 45%). The synthesis of large quantities of **2i** was performed as follows: A nitrogen filled 250 mL Schlenk flask was loaded with pyromellitic dianhydride (57.31 mmol, 1.0 eq). It was then gently heated under vacuum and refilled with nitrogen. This was repeated 3 times. Afterwards, acetic acid (115 mL) and 2-(2-(2-methoxyethoxy)ethoxy)ethylamine (57.31 mmol, 1.0 eq) were injected. The flask was heated for 24 h to 120 °C. Then, 2-pentylamine (57.31 mmol, 1.0 eq) were injected. The mixture was heated another 24 h to 120 ºC. After cooling down, the mixture was neutralized with sodium bicarbonate and extracted with DCM/MeCN (5/1). The organic phase was washed again with sodium carbonate and demi water and dried over $MgSO_4$ and concentrated. The residue was purified by column chromatography (silica gel, ethyl acetate/hexane 1/1) to yield a white gel, which solidifies after placing in the fridge (12.64 g, 51%). ^{1}H NMR (400 MHz, Chloroform-*d*) δ 8.23 (s, 2H), 4.44 – 4.37 (m, 1H), 3.95 (t, J = 5.6 Hz, 2H), 3.77 (t, J = 5.7 Hz, 2H), 3.68 – 3.63 (m, 2H), 3.61 – 3.55 (m, 4H), 3.50 – 3.46 (m, 4H), 3.33 (s, 3H), 2.10 – 2.01 (m, 1H), 1.77 – 1.69 (m, 1H), 1.49 (d, J = 6.9 Hz, 3H), 1.33 – 1.21(m, 2H), 0.91 (t, J = 7.4 Hz, 3H). ^{13}C NMR (100 MHz, Chloroform-*d*) δ 166.36, 166.17, 137.15, 137.07, 118.05, 71.86, 70.57, 70.57, 70.53, 70.07, 67.62, 59.00, 48.07, 37.91, 36.67, 19.94, 18.56, 13.62. MS (MALDI) *m/z* calculated for $C_{24}H_{32}N_2NaO_{10}(M+Na)^+$: 455,1789, found 455.21.

Synthesis of **3b:** Prepared by General Procedure F using isopropylamine to yield white crystals (493 mg, 82% yield). ^{1}H NMR (400 MHz, Chloroform-*d*) δ 4.65 (septet, J = 6.9 Hz, 3H), 1.52 (d, J = 6.9 Hz, 18H). ^{13}C NMR (100 MHz, Chloroform-*d*) δ 162.54, 133.27, 44.65, 19.74. ^{1}H and ^{13}C NMR spectra are in agreement with literature.[8,9]

Synthesis of **3c:** Prepared by General Procedure G using 2-pentylamine to yield white crystals (216 mg, 50% yield). ^{1}H NMR (400 MHz, Chloroform-*d*) δ 4.56 – 4.47 (m, 3H), 1.50 (d, J = 7.0 Hz, 9H), 1.46 – 1.19 (m, 12H), 0.90 (t, J = 7.3 Hz, 9H). ^{13}C NMR (100 MHz, Chloroform-*d*) δ 162.77, 133.22, 48.87, 35.35, 19.96, 13.60. MS (MALDI) *m/z* calculated for $C_{27}H_{33}N_3NaO_6(M+Na)^+$: 518.2262, found 518.24.

Synthesis of **3d:** Prepared by General Procedure G using 2-ethyl-1-hexylamine, purified by filtration over silica gel to yield white crystals (164 mg, 18% yield). ^{1}H NMR (400 MHz, Chloroform-*d*) δ 3.70 (d, J = 7.2 Hz, 6H), 3.70 (quintet, J = 6.3 Hz, 3H), 1.40 – 1.22 (m, 24H), 0.95 – 0.85 (m, 18H). ^{13}C NMR (100 MHz, Chloroform-*d*) δ 162.82, 133.31, 43.15, 38.21, 30.65, 28.59, 23.94, 22.90, 14.05, 10.38. ^{1}H and ^{13}C NMR spectra are in agreement with literature.[7]

Synthesis of **3e:** Prepared by General Procedure F using 2-methoxyethylamine to yield white crystals (141 mg, 21% yield). ^{1}H NMR (400 MHz, Chloroform-*d*) δ 4.03 (t, J = 5.4 Hz, 6H), 3.70 (t, J = 5.4 Hz, 6H), 3.33 (s, 9H). ^{13}C NMR (100 MHz, Chloroform-*d*) δ 162.34, 133.43, 68.55, 58.58, 38.42. MS (MALDI) *m/z* calculated for $C_{21}H_{21}N_3NaO_9(M+Na)^+$: 482.1170, found 482.16.

Synthesis of **3f:** Prepared by General Procedure G using 2-(2-methoxyethoxy)ethylamine to yield white crystals (233 mg, 27% yield). ^{1}H NMR (400 MHz, Chloroform-*d*) δ 4.04 (t, J = 7.0 Hz,6H), 3.82 (t, J = 7.0 Hz,6H), 3.48 (t, J = 7.0 Hz, 6H), 3.30 (s, 9H). ^{13}C NMR (100 MHz, Chloroform-*d*) δ 162.28, 133.39, 71.85, 69.88, 67.23, 58.97, 38.36.MS (MALDI) *m/z* calculated for $C_{27}H_{33}N_3NaO_{12}(M+Na)^+$: 614.1956, found 614.24.

Synthesis of **3g:** Prepared by General Procedure G using 2-(2-(2-methoxyethoxy)ethoxy)ethylamine to yield a brown gel (213 mg, 20% yield). ^{1}H NMR (400 MHz, Chloroform-*d*) δ 4.02 (t, J = 5.6 Hz, 6H), 3.81 (t, J = 5.6 Hz, 6H), 3.66 – 3.63 (m, 6H), 3.60 – 3.55 (m, 12H), 3.50 – 3.46 (m, 6H), 3.32 (s, 9H). ^{13}C NMR (100 MHz, Chloroform-*d*) δ 162.33, 133.43, 71.86, 70.57, 70.50, 70.08, 58.99, 50.70, 38.47. MS (MALDI) *m/z* calculated for $C_{33}H_{45}N_3NaO_{15}(M+Na)^+$: 746.2743, found 746.35.

Synthesis of **3h:** Prepared by General Procedure G using 2-(2-(2-(2-methoxyethoxy)ethoxy)ethoxy)ethylamine to yield a brown gel (212 mg, 17% yield). ^{1}H NMR (400 MHz, Chloroform-*d*) δ 4.02 (t, J = 5.6 Hz, 6H), 3.81 (t, J = 5.6 Hz, 6H), 3.67 – 3.63 (m, 12H), 3.61 – 3.59 (m, 18H), 3.53 – 3.49 (m, 6H), 3.35 (s, 9H). ^{13}C NMR (100 MHz, Chloroform-*d*) δ 162.28, 133.35, 71.86, 70.49, 70.49, 70.47, 70.39, 69.98, 67.19, 58.94, 38.39.

Synthesis of N-(ferrocenylmethyl)-*N,N*-dimethylethanaminium hexafluorophosphate**:** A 250 mL flask was loaded with (dimethylaminomethyl)ferrocene (10 g, 41.13 mmol, 1.0 eq), dichloromethane (20.6 mL), bromoethane (9.15 mL, 123.39 mmol, 3.0 eq), and stirred for 3 hours at room temperature. After concentration under high vacuum, 10 mL of saturated potassium hexafluorophosphate solution were added and three times extracted with DCM/MeCN (5/1). The organic phase was twice washed saturated potassium hexafluorophosphate solution and once with demi water. After drying over $MgSO_4$ and concentration, the residue was purified by recrystallization from methanol to yield orange crystals (13.75 g, 80% yield). ^{1}H NMR (400 MHz, Chloroform-*d*) δ 4.44 – 4.39 (m, 4H), 4.34 (s, 2H), 4.27 (s,5H), 3.26 (quartet, J = 7.3 Hz, 2H), 2.92 (s, 6H), 1.38 (t, J = 7.3 Hz, 3H).^{13}C NMR (100 MHz, Chloroform-*d*) δ 71.93, 71.68, 70.73, 69.63, 65.60, 58.66, 48.70, 8.16. MS (MALDI) *m/z* calculated for $C_{15}H_{22}FeN$ $(M–PF_6)^+$: 272.1096, found 272.12.

Synthesis of ***N*-(ferrocenylmethyl)-*N,N*-dimethylethanaminium bis(trifluoromethane-sulfonyl)imide:** A 250 mL flask was loaded with (dimethylaminomethyl)ferrocene (10 g, 41.13 mmol, 1.0 eq), dichloromethane (20.6 mL), bromoethane (9.15 mL, 123.39 mmol, 3.0 eq), and stirred for 3 hours at room temperature. After concentration under high vacuum, 10 mL of a 5 M solution of lithium bis(trifluoromethanesulfonyl)imide in water were added and three times extracted with DCM/MeCN (5/1). The organic phase was once extracted with a saturated aqueous lithium bis(trifluoromethanesulfonyl)imide solution and once with demi water. After drying over $MgSO_4$ and concentration, the residue was purified by recrystallization from methanol to yield red-brown crystals (15.1 g, 68% yield). ^{1}H NMR (400 MHz, Chloroform-*d*) δ 4.48 (s, 2H), 4.43 – 4.37 (m, 4H), 4.28 (s,5H), 3.37 (quartet, J = 7.3 Hz, 2H), 2.92 (s, 6H), 1.41 (t, J = 7.3 Hz, 3H).^{13}C NMR (100 MHz, Chloroform-*d*) δ 71.81, 71.46, 70.87, 69.60, 66.03, 58.63, 48.86, 8.28. MS (MALDI) *m/z* calculated for $C_{15}H_{22}FeN$ $(M–TFSI)^+$: 272.1096, found 272.13.

Electrochemistry and battery cycling experiments

General remarks

Acetonitrile (99.9%, Extra Dry over Molecular Sieve, AcroSeal™) was obtained from ACROS Organics and used as received. Tetrabutylammonium hexafluorophosphate ($TBAPF_6$) (≥99.0%, for electrochemical analysis) was obtained from Sigma-Aldrich and *N*-ethyl-*N,N*-dimethyl-*N*-(2-methoxyethyl)ammonium bis(fluorosulfonyl)imide ($N_{112.1O2}FSI$) (99.9%) from Solvionic. 0.2 M stock solutions of both supporting electrolytes in acetonitrile were prepared in a glovebox. Fumasep® FAP-375-PP and Fumasep® FAA-3-50 membranes were obtained from Fumatech and ion-exchanged in saturated KPF_6 and KFSI solutions, respectively, washed with water and then dried under high vacuum at 70 °C before use.

Cyclic voltammetry

All the cyclic voltammetry measurements were performed in a nitrogen-filled glovebox with a Biologic VSP potentiostat using a three-electrode electrochemical cell, consisting of a glassy carbon disk working electrode (0.07 cm^2, BASi), a Ag/Ag^+ quasi-reference electrode (BASi) with 0.01 M $AgBF_4$(Sigma) in acetonitrile, and a platinum wire counter electrode. All experiments were run in the 0.2 M $TBAPF_6$ or $N_{112.1O2}FSI$ stock electrolyte solutions. Ferrocene (1 – 10 mM) was used as an internal reference.

The determination of the diffusion coefficients was accomplished by varying the scan rate of the cyclic voltammetry measurements between 10 and 640 mV/s. By plotting the cathodic and anodic peak height currents vs. the square root of the scan rate showed a linear relationship which indicates a transport limited redox process (Figure S5). The slope of this linear relation was used in the Randles-Ševčik equation (S1) to determine the diffusion coefficients.

$$i_p = 0.4463 \cdot nFAC\sqrt{\frac{nFvD}{RT}} \qquad \text{(S1)}$$

With i_p the peak current in A, n the number of electrons transferred, F the Faraday constant in C/mol, A the area of the electrode in cm^2, C the concentration of redox active species in mol/cm^3, D the diffusion coefficient in cm^2/s, v the scan rate in V/s, R the gas constant in J/(mol·K), and T the absolute temperature in K.

Heterogeneous electron transfer rates were determined following the Nicholson method.[10] Briefly, the peak separations (ΔE_p) between the cathodic and anodic peaks depend on the scan rate. Thus, they were determined at various scan rates and fitted to a working curve to obtain the dimensionless parameter Ψ. Plotting the resulting values of Ψ vs. the inverse of the scan rate (Figure S6) gave a linear relationship of which the slope is used to determine k_0 according to:

$$\Psi = \frac{\gamma k_0}{\sqrt{\pi n F v D / RT}} \quad \text{(S2)}$$

where $\gamma = D/D'$ the ratio of the diffusion constants for the reduction and re-oxidation.

Bulk electrolysis

All bulk electrolysis charge/discharge measurements were carried out in a nitrogen-filled glovebox with a Biologic VSP potentiostat in a custom glass H-cell with a P5 porous glass frit. For the electrodes, reticulated vitreous carbon (100 ppi, ≈70 cm^2 surface area) was used. The working side of the H-cell was equipped with an additional Ag/Ag^+ quasi-reference electrode (BASi) with 10 mM $AgBF_4$. The electrolyte contained 5 – 50 mM anolyte and 0.2 M $TBAPF_6$ or $N_{112.1O2}FSI$ and with additional 1.5 equivalent ferrocene or ferrocenium per redox event to prevent solvent oxidation at the counter electrode. Both chambers of the H-cell were loaded with 5 mL electrolyte solution and stirred continuously during galvanostatic cycling at a current of 5 mA. Voltaic cutoffs where set depending on the redox potentials of the compound.

Symmetric H-cell cycling

The cycling was carried out in a nitrogen-filled glovebox with a Biologic VSP potentiostat. A 10 mM solution of reduced **2i** in 200 mM $TBAPF_6$/acetonitrile was prepared in a bulk electrolysis. The fully reduced solution was removed and mixed with an equal amount – in this case 5.5 mL – of a 10 mM neutral **2i** solution, yielding a starting solution at 50% SOC. This was equally divided over the compartments of a fresh H-cell. By applying a positive current over the electrodes of the H-cell (positive polarization), the solution in one compartment is re-oxidized towards 0% SOC while the other one is further reduced towards 100% SOC. Applying a negative current (negative polarization) results in reversal of the SOCs between the compartments. This represents one cycle in the symmetric H-cell cycling. Both compartments were stirred. The cutoff potentials were ±1 V and the charging rate ±1 mA.

Symmetric flow cell cycling

The cycling was carried out in a nitrogen-filled glovebox with a Biologic VSP potentiostat. 11 mL of a 50% SOC solution containing diimide **2i** in a concentration of 100 mM with 300 mM $TBAPF_6$ in acetonitrile was prepared as described of symmetric H-cell cycling and equally spread over the two compartments of the flow setup to investigate the stability of **2i** at increased concentration in a flow battery setup (see detailed description of the setup below). An anion exchange membrane (Fumasep FAA-3-50) was used as separator. The flow rate was 10 mL/min, the cutoff potentials ±1 V and the charging rate ±12.75 mA.

Redox flow battery

Measurements under flow conditions were carried out using a zero-gap flow cell.[11] The battery was assembled outside the glovebox. A combination of a graphite charge-collecting plate and two layers of a non-woven carbon felt electrode with an area of 2.55 cm^2 (Sigracet 29AA) was put on either side of the flow cell. A ±10% compression of the felt was achieved by the use of Gore-tex ePTFF gaskets. The two halve cells were separated by either a Fumasep® FAP-375-PP or Fumasep® FAA-3-50 anion-exchange membrane. The gasket window provided for an exposed area of the membrane which was used as the active area of the flow cell. The cell was connected to a peristaltic pump (Cole-Parmer) by Masterflex C-flex ultra-pump tubing using a flow rate of 10 mL/min. The catholyte and anolyte reservoirs were filled with 6 mL of a solution of redox materials and electrolyte salt in the reported concentrations. Before starting the measurement, the cell was pretreated by flowing the solution through the cell for 30 minutes. Once the membrane was fully wetted as evidenced by impedance measurements, the cycling was started. A galvanostatic charge/discharge cycling was performed using currents of ±10 mA/cm^2 for the mixed battery shown in Figure 6 with potential cutoffs at +2.6 V and 0 V and 7.5 mA/cm^2 with additional voltaic holds at 3 V and 0 V to maximize material utilization for the non-mixed battery shown in Figure S17. Potentiostatic electrochemical impedance spectroscopy (PEIS) measurements were performed at various stages of charge from 500 kHz to 50 Hz using a 10 mV sine perturbation. A polarization measurement was collected at full SOC and ranging from -25.5 to -400 mA. The energy efficiency (EE) of this multi-electron battery was determined by the ratio of the time-integrated output and input power density during discharging and charging over each cycle. The voltage efficiency (VE) is then determined from EE by dividing by CE.

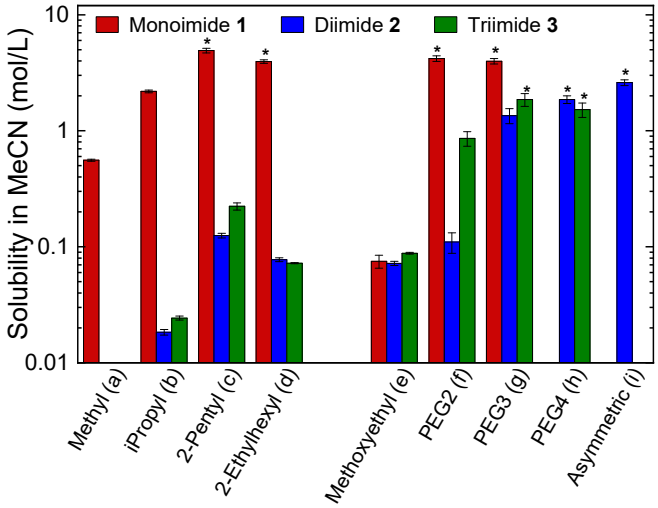

Figure S1. Solubility of compounds **1a–h**, **2b–i**, and **3b–h** in MeCN. Bars with an asterisk represent (viscous) liquids at room temperature. Note the logarithmic scale.

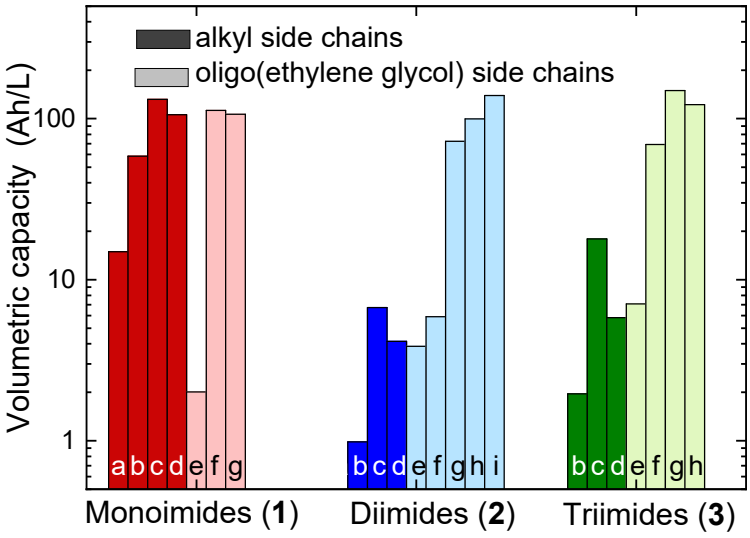

Figure S2. Volumetric capacity of **1a–g**, **2b–i**, and **3b–h** based on their solubility as neutral molecules in MeCN. Note the logarithmic scale.

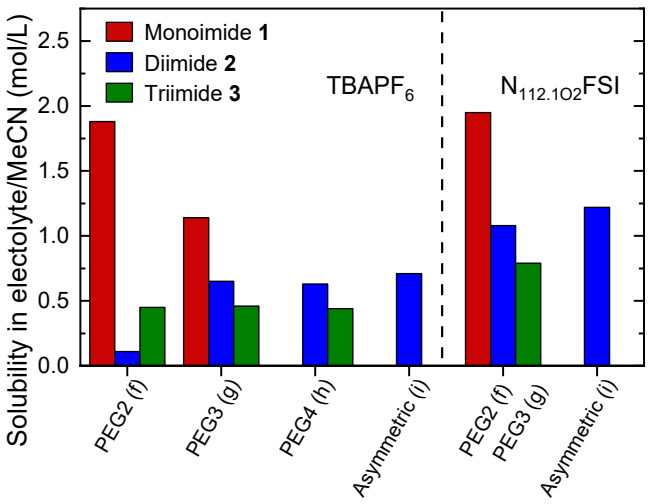

Figure S3. Solubility of compounds **1f–h**, **2f–i**, and **3f–h** in MeCN with one, two, or three equivalents of electrolyte salt ($TBAPF_6$ or $N_{112.1O2}FSI$) respectively.

Table S1. Reduction Potentials $E_{1/2}$ (V) of the Mono-, Di-, and Triimide Derivatives versus Fc/Fc^+.

Monoimides		Diimides			Triimides			
	1st		1st	2nd		1st	2nd	3rd
1a	−1.90							
1b	−1.93	**2b**	−1.29	−1.92	**3b**	−1.09	−1.72	−2.49
1c	−1.88	**2c**	−1.28	−1.92	**3c**	−1.07	−1.72	−2.50
1d	−1.91	**2d**	−1.26	−1.90	**3d**	−1.04	−1.70	−2.51
1e	−1.89	**2e**	−1.20	−1.81	**3e**	−1.02	−1.64	−2.35
1f	−1.88	**2f**	−1.23	−1.84	**3f**	−1.03	−1.64	−2.36
1g	−1.92	**2g**	−1.23	−1.85	**3g**	−1.02	−1.65	−2.37
		2h	−1.22	−1.84	**3h**	−1.02	−1.64	−2.35
		2i	−1.26	−1.88				

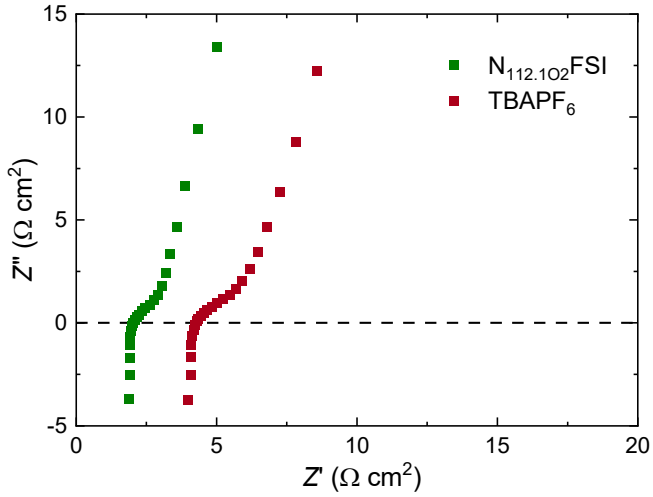

Figure S4. Potentiostatic electrochemical impedance spectroscopy (PEIS) in a flow cell with 0.2 M diimide **2i** and 0.4 M Fc1N112-FSI in 0.6 M of $N_{112.1O2}$FSI/MeCN (green squares) or 0.6 M of $TBAPF_6$/MeCN (red squares) using a Fumasep FAA-3-PE-30 membrane. The intersect with the *Z'*-axis represents the DC resistance originating from cables, membrane, and solution.

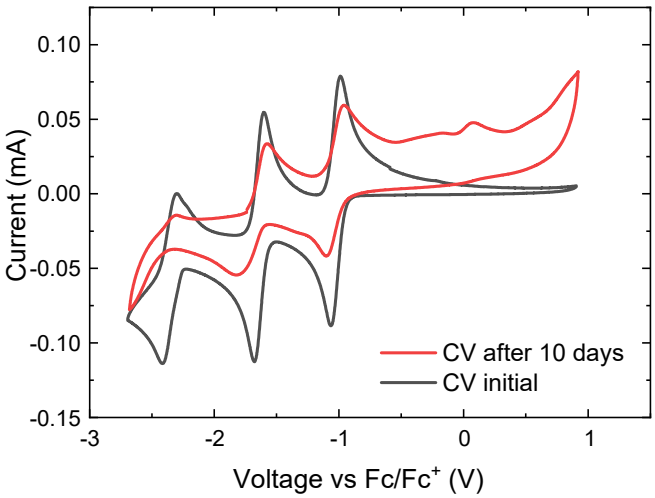

Figure S5. Cyclic voltammograms of a fresh solution of triimide **3f** (black line) in 200 mM $TBAPF_6$/MeCN and of the charged solution after 10-day storage in a nitrogen-filled glovebox (red line).

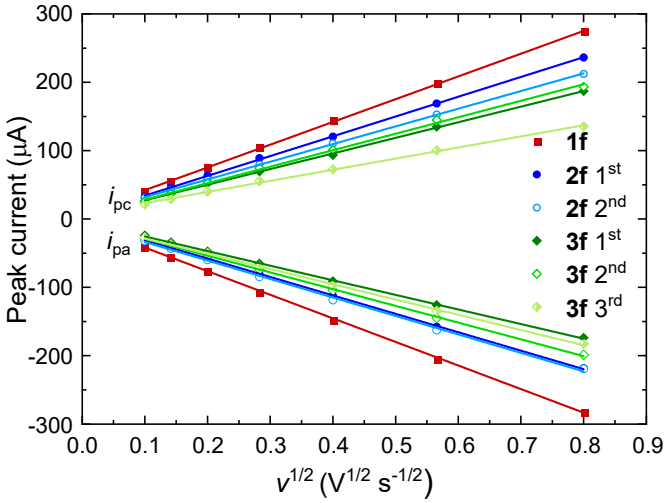

Figure S6. Peak currents (i_p and i_a) obtained from Figure 3 vs. $v^{1/2}$. The anodic peak currents were used to determine the diffusion coefficients listed in Table 1 for the successive single-electron reduction steps of compounds **1f**, **2f**, and **3f**. Lines are least-squares fits to the data.

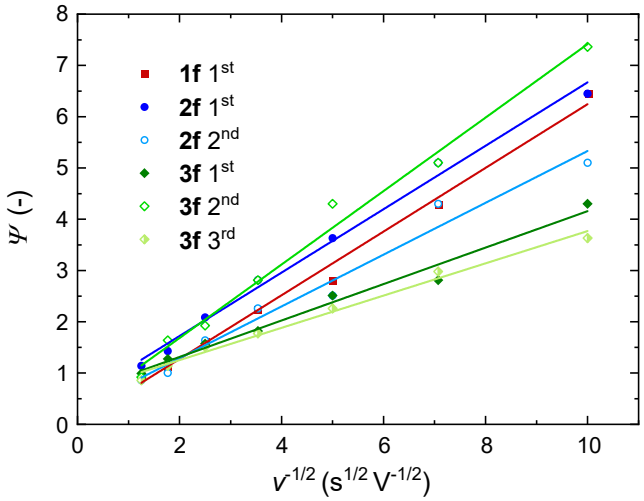

Figure S7. Ψ(see Equation (S2)) vs. $v^{-1/2}$ used to determine the electron transfer constants k_0 listed in Table 1 for the successive single-electron reduction steps of compounds **1f**, **2f**, and **3f**. Lines are least-squares fits to the data.

Figure S8 shows representative cycling curves of mono-, di-, and triimides **1f**, **2f**, and **3f** at 5 mM concentration. For these initial stability studies the imide anolytes were mixed with 1.5 equivalents of *N*-(ferrocenylmethyl)-*N*,*N*-dimethylethanaminium hexafluorophosphate ($Fc1N112PF_6$) per electron as catholyte to have a controlled oxidation reaction at the counter side and preempt the formation of highly reactive species which can crossover from the anolyte side.[12] $Fc1N112PF_6$ exhibits a chemically reversible oxidation at $E_{1/2}$ = 0.23 V vs. Fc/Fc^+. A critical look on the cycling performance of monoimide **1f** and diimide **2f** shows a slightly enhanced cycling stability of the latter one (Figure S8a). In contrast, triimide **3f** degraded very fast within the first 7 cycles to about one third of its capacity after which the capacity decayed somewhat slower than the other two compounds. Looking at the charge-discharge curves of **3f** (Figure S8d) reveals additional potential steps apart from the three expected redox events, indicating the formation of new redox active degradation products after the first cycles. Formation of degradation products is not observed in Figure S8b and Figure S8c for **1f** and **2f**.

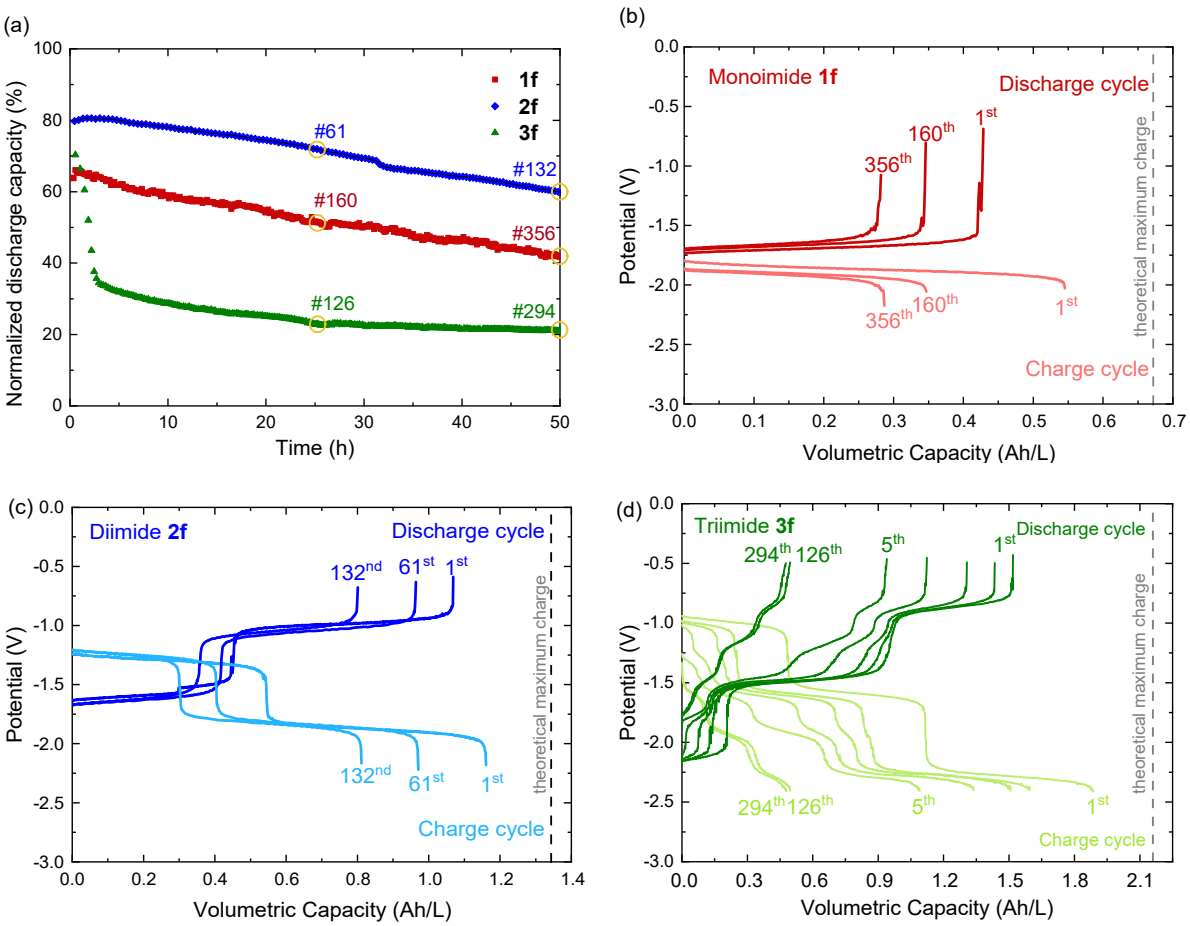

Figure S8. (a) Discharge capacity normalized by the theoretical maximum capacity versus time for one-, two-, and three-electron charge-discharge bulk electrolysis in an H-cell containing 5 mM acetonitrile solutions of **1f** (red), **2f** (blue), and **3f** (green) containing 0.2 M $TABPF_6$ electrolyte and 1.5 eq of $Fc1N112PF_6$ per transferable electron of the anolyte. (b-d) Charge-discharge curves of the first cycle, the cycle after 25 h, and the last cycle for **1f**, **2f**, and **3f**. For **3f** the second till fifth cycles are also depicted.

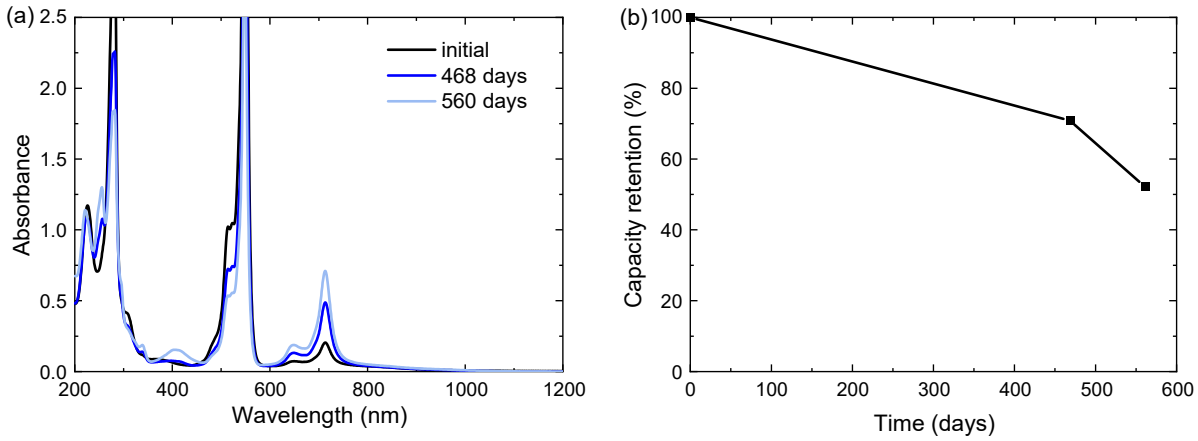

Figure S9. (a) UV-vis-NIR spectra of a charged solution of 50 mM of diimide **2e** at 10 times dilution in 200 mM $TBAPF_6$/MeCN at different points in time. (b) Capacity retention of **2e** in 200 mM $TBAPF_6$/MeCN over 560 days. The capacity was determined at a wavelength of 514 nm. An average loss of capacity of less than 1.7% per 20 days was determined by taking the lost charge after 560 days.

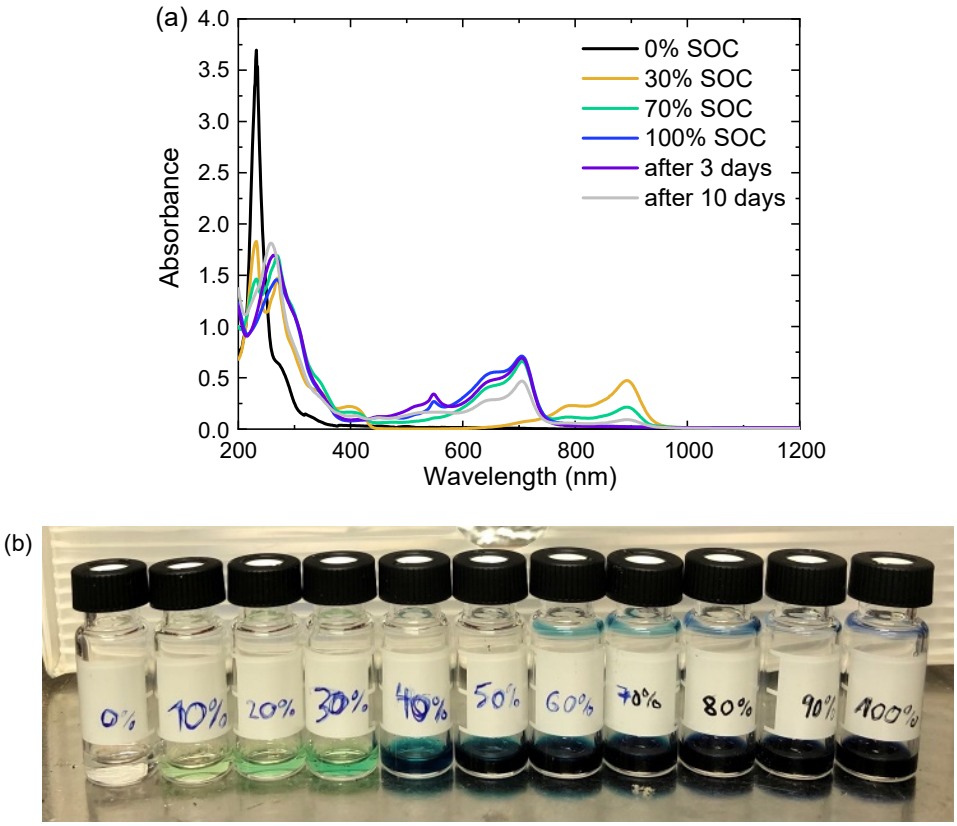

Figure S10. (a) UV-vis-NIR spectra of a charged solution of 5 mM of triimide **3f** in 200 mM $TBAPF_6$/MeCN at different SOCs and after several days of storing in a nitrogen-filled glovebox. (b) Samples of triimide **3f** at different SOC.

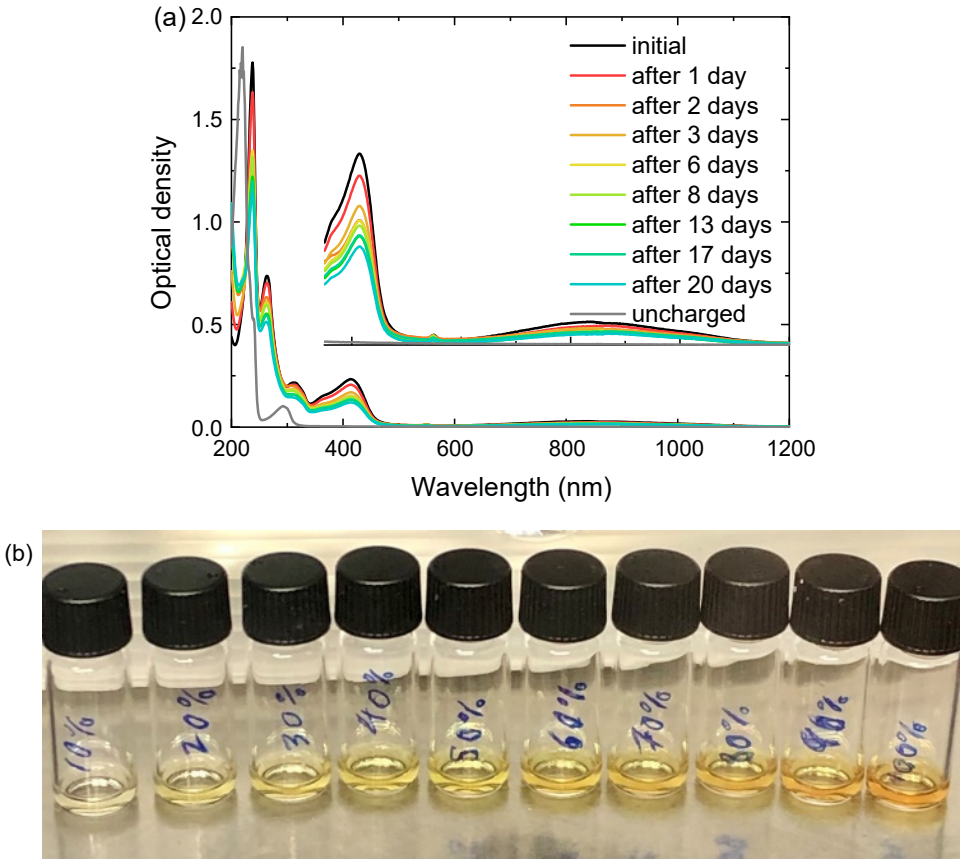

Figure S11. (a) UV-vis-NIR spectra of a 5 mM solution of monoimide **1f** in 200 mM $TBAPF_6$/MeCN uncharged (grey) and charged at several points in time. (b) Samples of monoimide **1f** at different SOC.

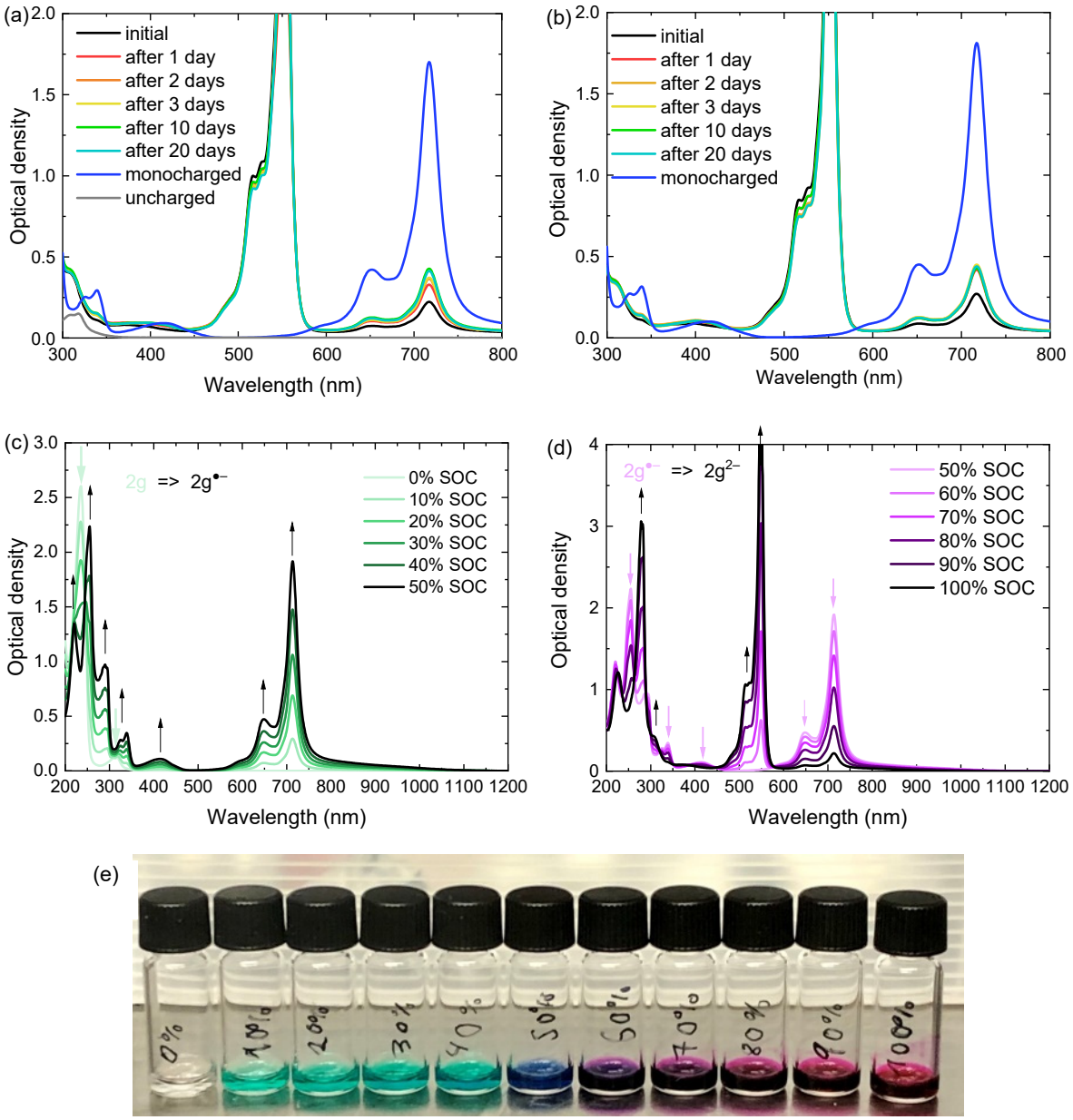

Figure S12. UV-vis-NIR spectra of a 5 mM solution of diimide **2g** (a) and **2i** (b) in 200 mM $TBAPF_6$/MeCN uncharged (grey), monocharged (blue) and double charged at several points in time. (c) Reduction of **2g** to $\mathbf{2g}^{\bullet-}$. (d) Reduction of $\mathbf{2g}^{\bullet-}$ to $\mathbf{2g}^{2-}$ (e) Samples of diimide **2g** at different SOCs.

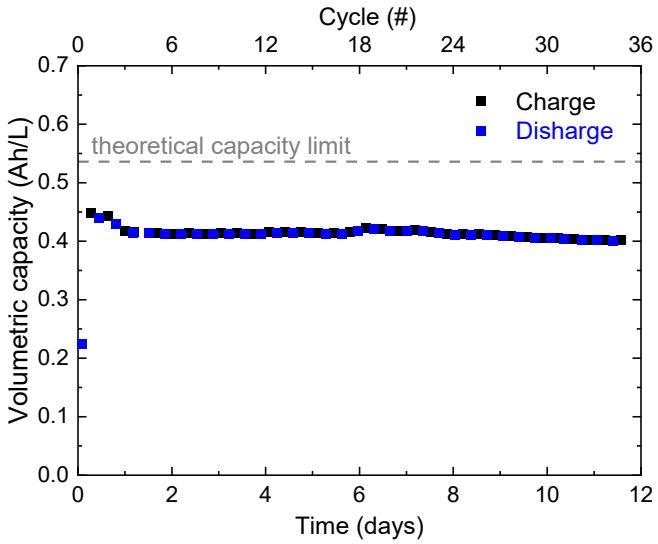

Figure S13. Volumetric charge-discharge capacity versus time of the symmetric H-cell cycling of 10 mM diimide **2i** in 200 mM $TBAPF_6$/MeCN. The dashed line represents the maximum theoretical capacity. The solution was prepared in a bulk electrolysis experiment. It was fully charged, mixed with the same amount of uncharged solution, and equally spread on the compartments of a fresh H-cell.

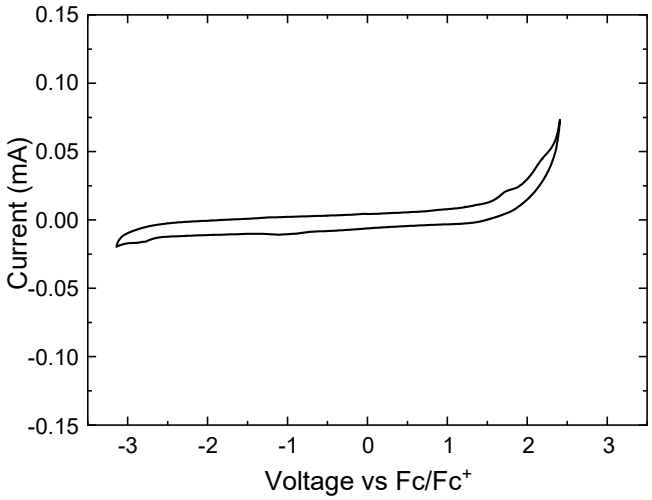

Figure S14. Electrochemical potential window of 100 mM $N_{112.1O2}FSI$ in acetonitrile at a scan rate of 100 mV/s.

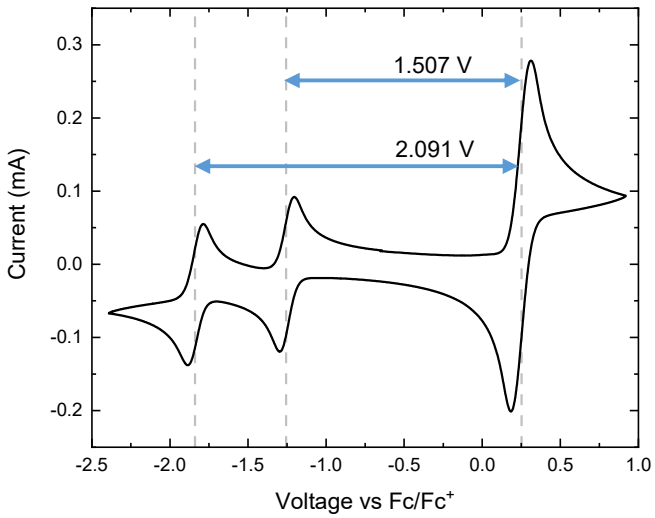

Figure S15. Initial CV measurement of the battery shown in Figure 6 at 50 times dilution at a scan rate of 100 mV/s. The concentrations are approximately 5 mM diimide **2i** and 12 mM Fc1N112-TFSI in 200 mM of $N_{112.1O2}$FSI /MeCN.

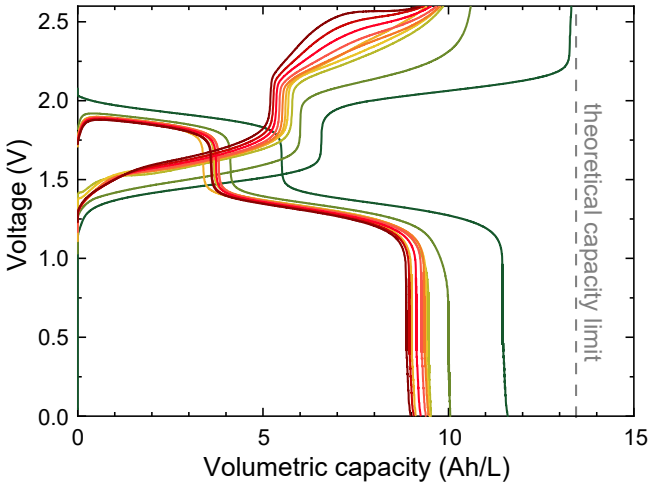

Figure S16. Voltage versus volumetric capacity curves with ascending cycle number from green to red for the flow cell cycling experiments shown in Figure 6. The dashed line represents the maximum theoretical capacity.

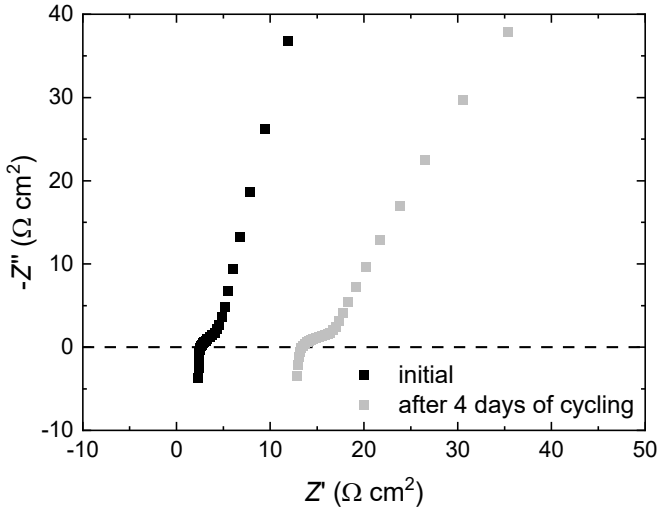

Figure S17. PEIS measurement of the flow cell cycling with 0.25 M diimide 2i and 0.6 M Fc1N112-TFSI in 0.6 M of $N_{112.1O2}$FSI/MeCN (cycling shown in Figure 6) using a Fumasep FAA-3-50 membrane before and after cycling for 4 days.

Table S2. Comparison of this Work with Reported Non-Aqueous Redox Flow Batteries.

Electrolytes	Concentration of transferable electrons (M)	Energy density (Wh/L)	Capacity loss rate (%/cycle, %/day) based on discharge capacity	CE, EE (%)	Maximum power density (mW/cm^2)
MePh|DBMMB[13]	0.3	9.3	0.1*, 10**	90, 69	120
BzNSN|DBMMB[14]	0.5 1	8 23.6*	0.39*, 8.3** 1.6*, 30**	94, 72 89, 48	120
NMePh|DMFc[15]	0.5	9.26	0.13, 34*	91, 60	41*
PTIO[16] (amphoteric)	0.5	9	1.4*, 400**	90, 60	29*
BuPh|DMFc[17]	0.1 1.0	2.41 24.1	0.06*, 30** >2.5**, >133**	94, 50 83, 45	131 192
BuPh|DFDE[18] (multi-electron)	0.9	21.7*	0.5**, 60**,≠	79, 61	37* 80* (0.1 M)
AB|Fc[19] (multi-electron)	0.8	14.9*	0.26, 3.8*	93, 56**	170
2-MBP|DBMMB[20]	0.1	8*	0.33*, 8.3**	95, 70	22*
BMEPZ|FL[21] (multi-electron)	0.8	17	0.63*, 2.63**	82, 60	36*
FcNTFSI|MVTFS[22] (multi-electron)	0.2	5.7	0.11, 9.5**	92, 73	56*
This work	0.5 1.0	12.1 24.1	0.8 and 4.2 5 and 12.1	97, 72 99.4, 34#	160 45

* Calculated using the data provided in the reference.

** Calculated using the data provided in the reference and additional assumptions/interpretation.

≠ Charge and discharge capacity show significant difference; decay for charge capacity is higher by a factor of 2

Average value, significant differences between the cycles

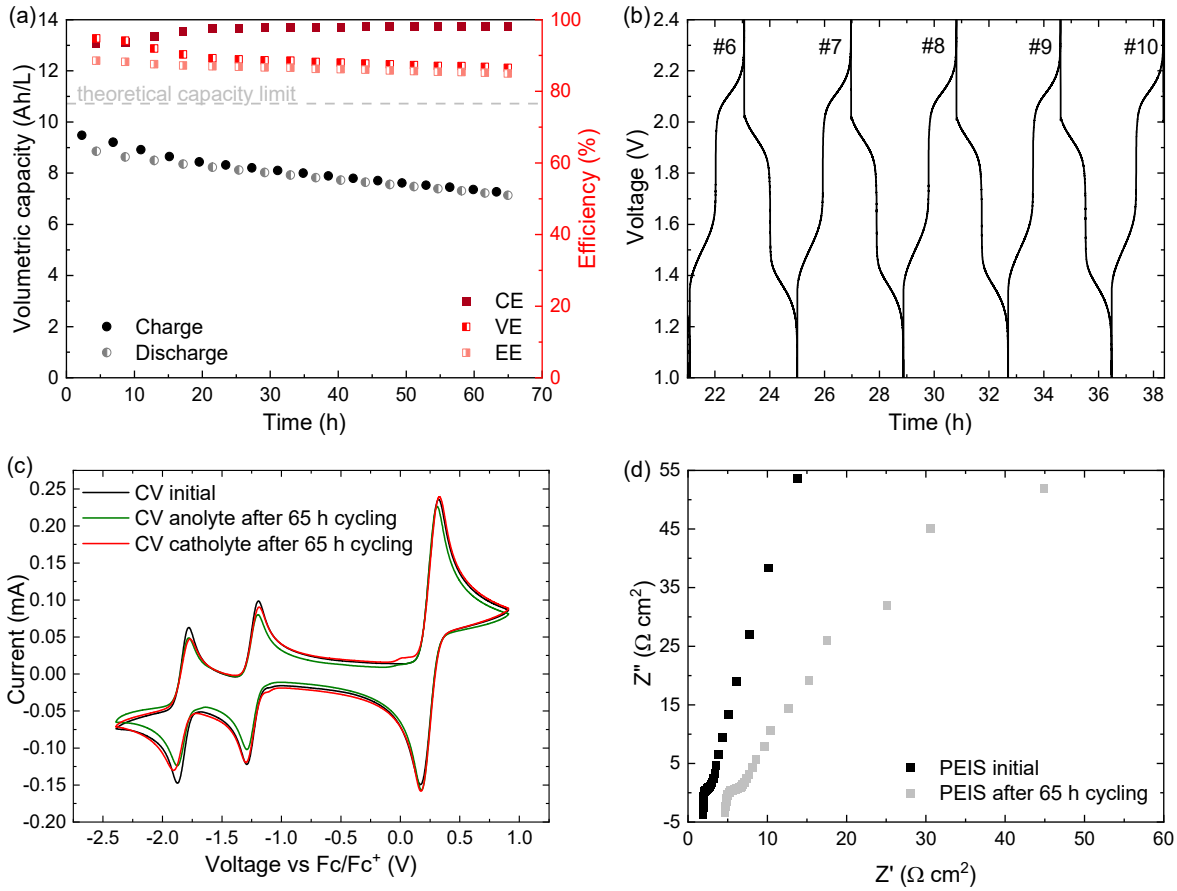

Figure S18. Mixed flow cell cycling of 0.2 M of diimide **2i** and 0.4 M Fc1N112-FSI in 0.6 M of $N_{112.1O2}$FSI/MeCN using a Fumasep FAA-3-PE-30 membrane. (a) Charge-discharge capacity (black and grey) and coulombic efficiency (red) versus time. The dashed line represents the maximum theoretical capacity. (b) Voltage versus time curves for the cycles 5 to 10. (c) CV measurements before and after 65 h of flow cell cycling. (d) PEIS measurements before and after 65 h of flow cell cycling.

Table S3. Detailed analysis of the CV measurements shown in Figure S18c.

	Peak separation (mV) [a]			i_{pc}/i_{pa} [a]			Retention anolyte (%)	Retention catholyte (%)
	A_1	A_2	C	A_1	A_2	C		
Initial	99	97	150	1.05	0.90	0.86	100	100
Anolyte side after	100	100	132	1.03	0.92	0.89	86	99
Catholyte side after	105	141	154	1.01	0.88	0.89	96	101

[a] A_1 = first reduction wave of anolyte; A_2 second reduction wave anolyte; C oxidation wave catholyte.

Detailed analysis of the CVs before and after the cycling lead to the conclusion that the redox chemistries of anolyte and catholyte stay mostly unimpaired by the cycling. The very small bumps prior to the first reduction and oxidation peaks could point to protonation of the active materials. Only an apparent loss of anolyte material in the reservoir where the reduction takes place was observed, however this loss is lower than the observed capacity fade. A reason for the discrepancy between the CV measurements and the capacity fade could be the fact that CV is dependent on the concentration, which would likely have changed slightly during the 65 h cycling experiment as evidenced by a difference in solvent level between the two reservoirs

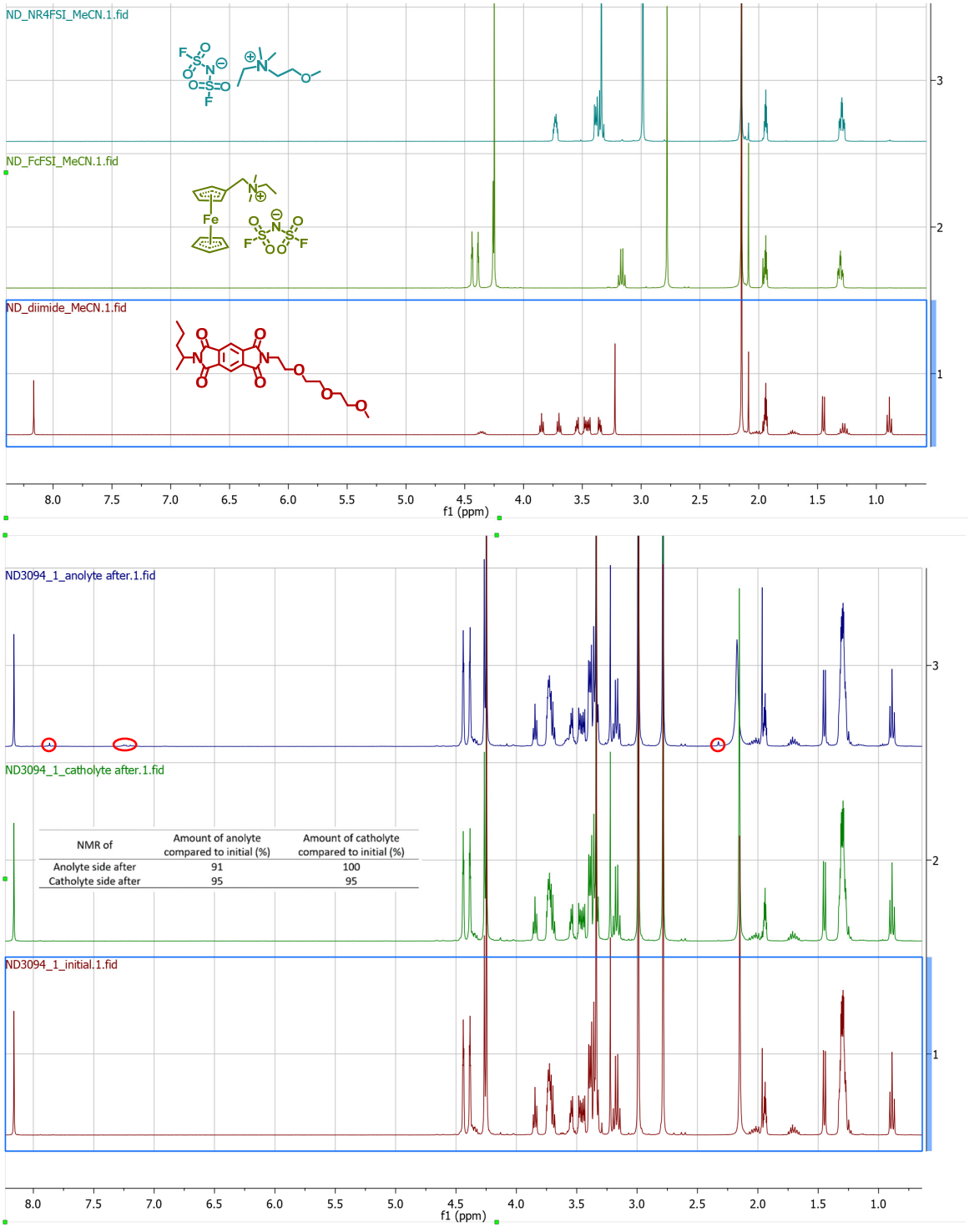

NMR of	Amount of anolyte compared to initial (%)	Amount of catholyte compared to initial (%)
Anolyte side after	91	100
Catholyte side after	95	95

Figure S19. NMR spectra of diimide **2i**, Fc1N112-FSI and $N_{112.1O2}$FSI in MeCN-d_3 as well as of the reservoir solutions of the battery shown in Figure S18 prior and after cycling. The red circles highlight the peaks that were not observed in the NMR spectra prior to cycling.

For the NMR samples, 50 µL were removed prior to cycling and of both reservoir after cycling. The solvent was evaporated and exactly 509 mg of MeCN-d_3 added to every sample. A careful comparison of the total amount of each compound based on the peak height, normalized to the signal of MeCN-d_3 at 1.94 ppm, reveals similar total loss of anolyte and catholyte over both reservoirs, however, the amount of catholyte is equally divided on both reservoirs while the anolyte loss only occurs on the side where the reduction takes place. This suggests that only the reduced anolyte and neutral catholyte species are crossing over through the membrane. This assumption coincides with the one observed with the CV measurements. A possible solution to minimize the loss could be the remixing of both reservoirs after several days/weeks.

Table S4. Comparison of different techniques regarding the capacity of the battery shown in Figure S18.

Technique	Amount of anolyte compared to initial on anolyte side (%)	Amount of catholyte compared to initial on catholyte side (%)
Capacity of battery	81 (no distinction possible)	
CV	86	101
NMR	91	95

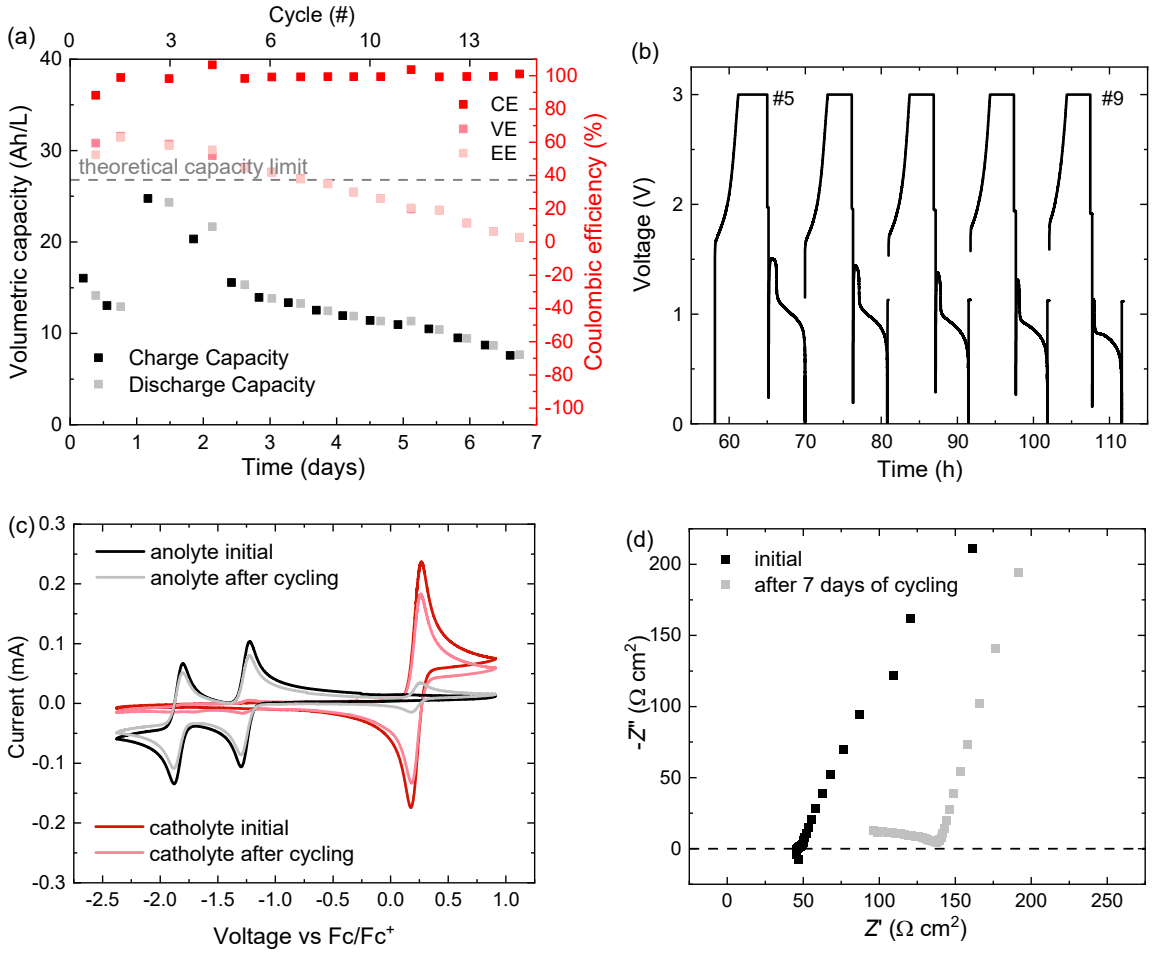

Figure S20. Non-mixed flow cell cycling of 0.5 M of diimide **2i** and 1.0 M Fc1N112-TFSI in 1.2 M of $N_{112,1O2}$FSI/MeCN using a Fumasep FAPQ-375-PP membrane. (a) Charge-discharge capacity (black and grey) and coulombic efficiency (red) versus time. The dashed line represents the maximum theoretical capacity. (b) Voltage versus time curves for the cycles 5 to 9. (c) CV measurements before and after one week of flow cell cycling. (d) PEIS measurements before and after flow cell cycling.

^{1}H and ^{13}C NMR spectra

1a

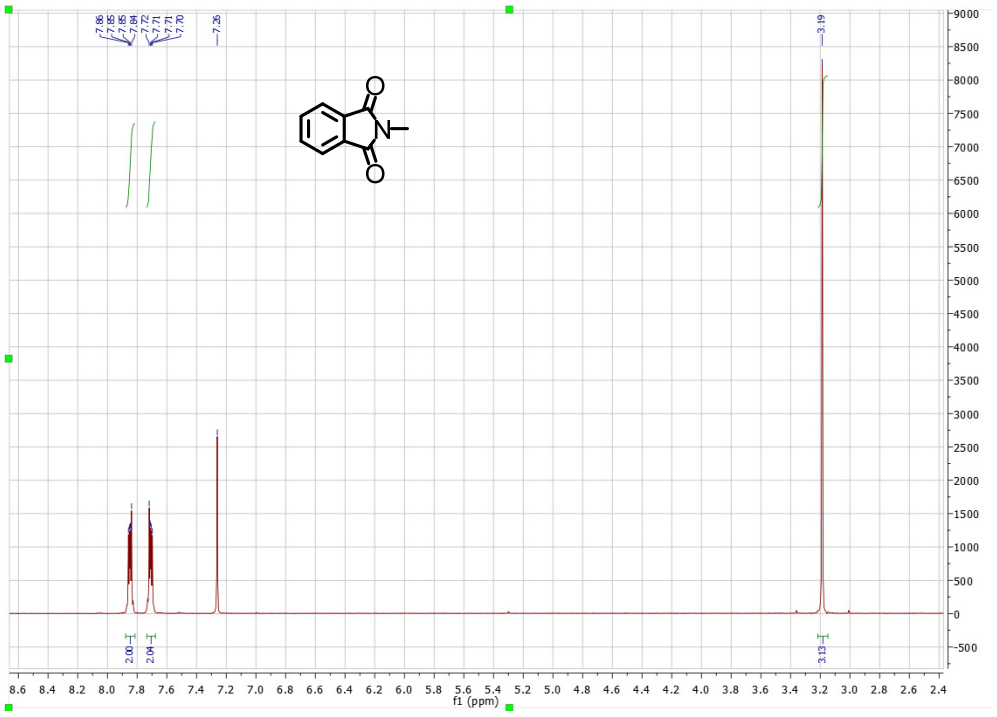

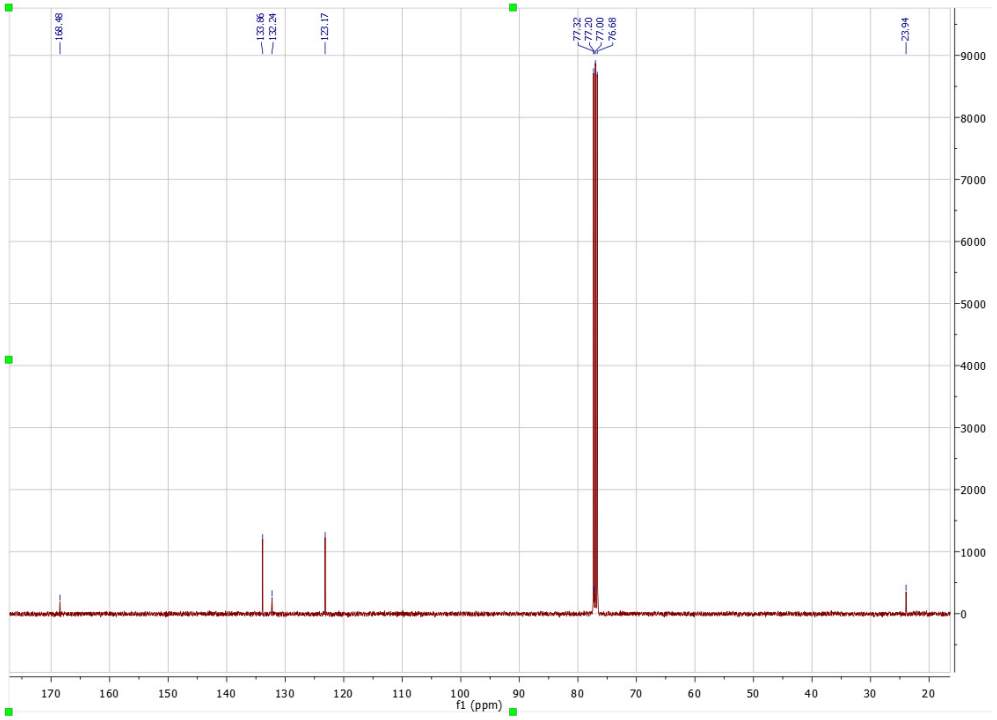

1b

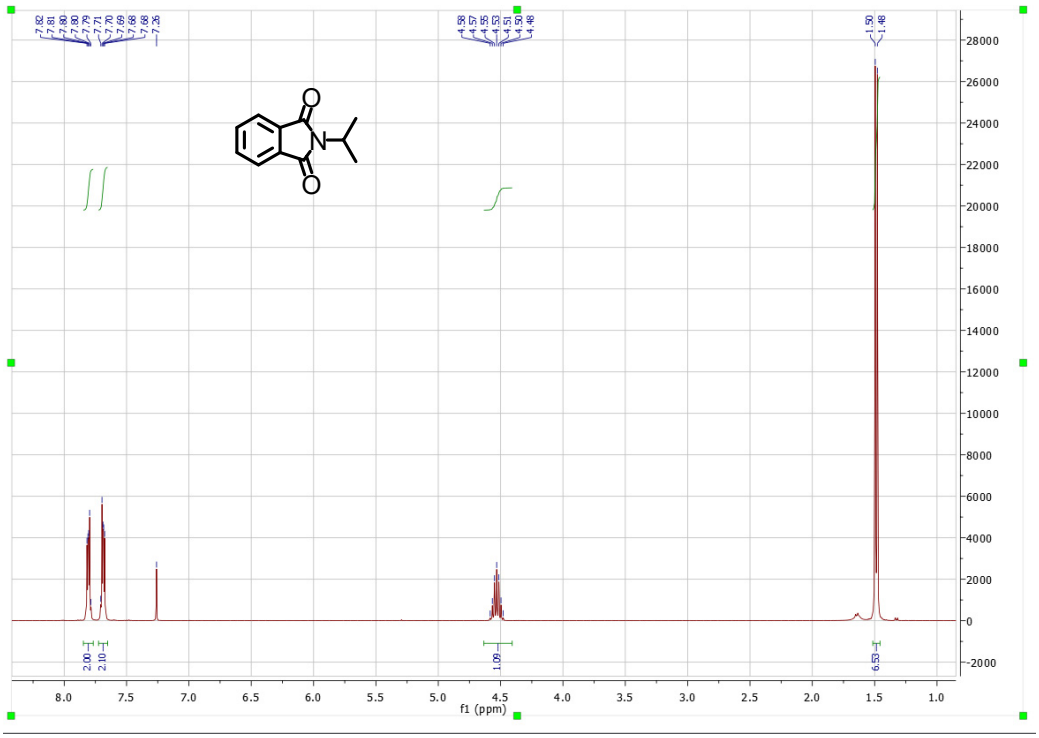
7.82
7.81
7.80
7.80
7.79
7.71
7.70
7.69
7.68
7.68
7.26
4.58
4.57
4.55
4.53
4.51
4.50
4.48
1.50
1.48
2.00
2.10
1.09
6.53
f1 (ppm)

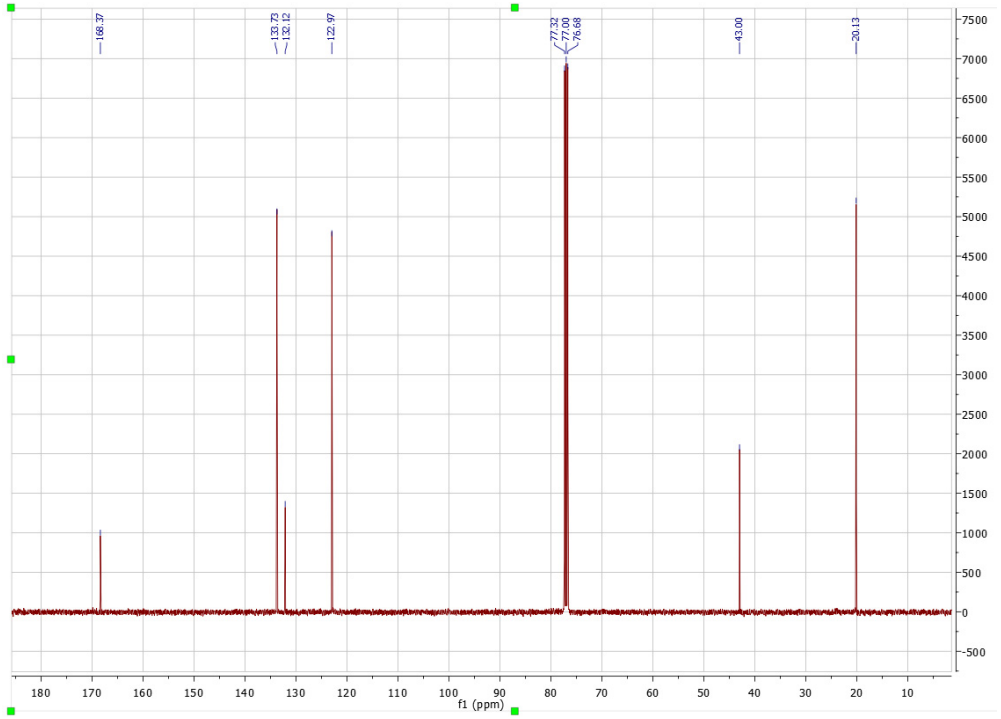
168.37
133.73
132.12
122.97
77.32
77.00
76.68
43.00
20.13
f1 (ppm)

1c

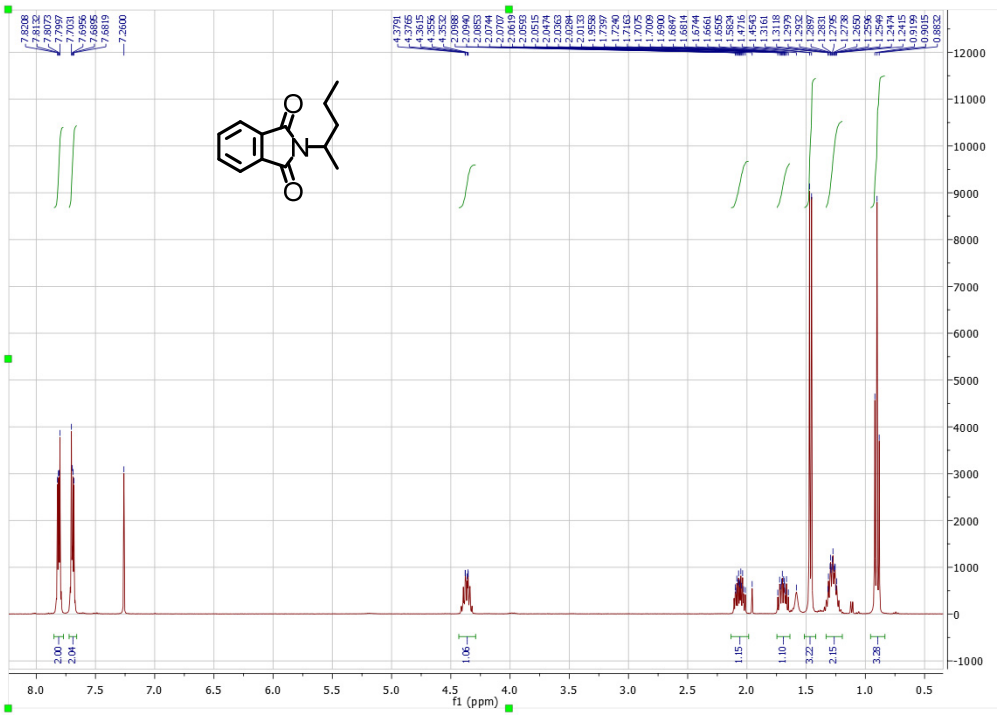

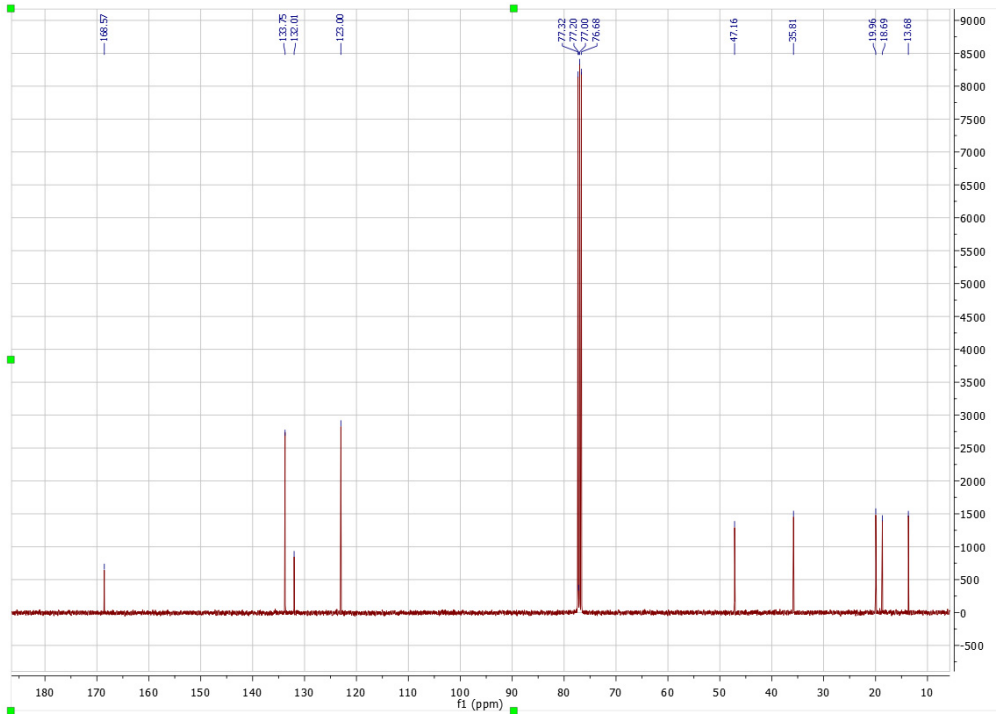

1d

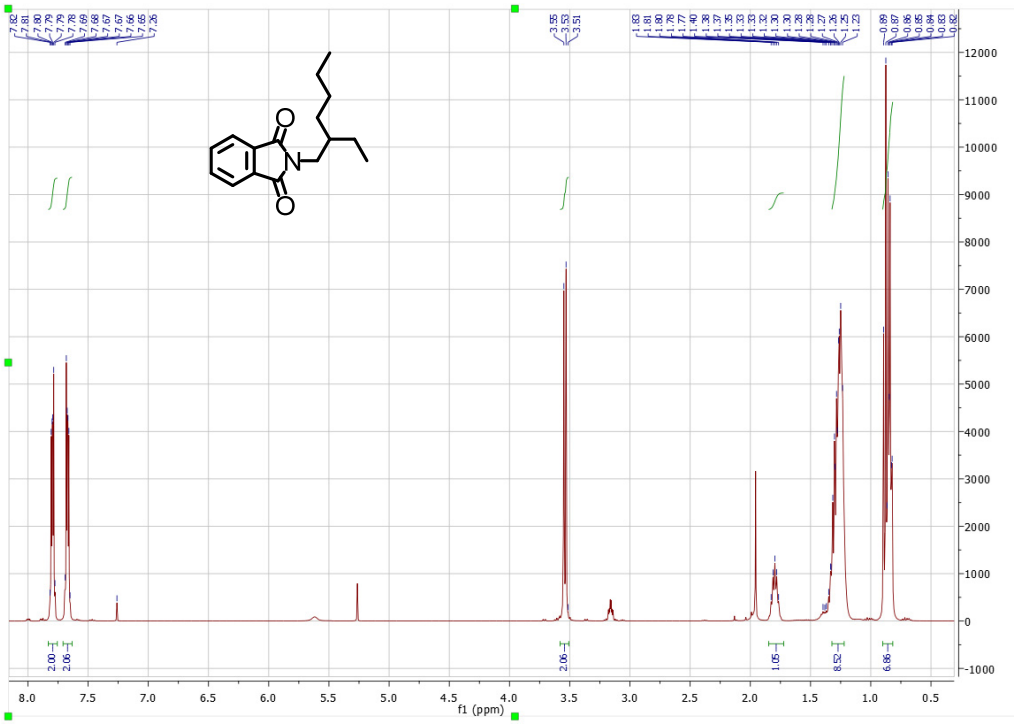
7.82
7.81
7.80
7.79
7.79
7.78
7.69
7.68
7.67
7.67
7.66
7.65
7.26
3.55
3.53
3.51
1.83
1.81
1.80
1.78
1.77
1.40
1.38
1.37
1.35
1.33
1.32
1.30
1.30
1.28
1.28
1.27
1.26
1.25
1.23
0.89
0.87
0.86
0.85
0.84
0.83
0.82
2.00
2.06
2.06
1.05
8.52
6.86
f1 (ppm)

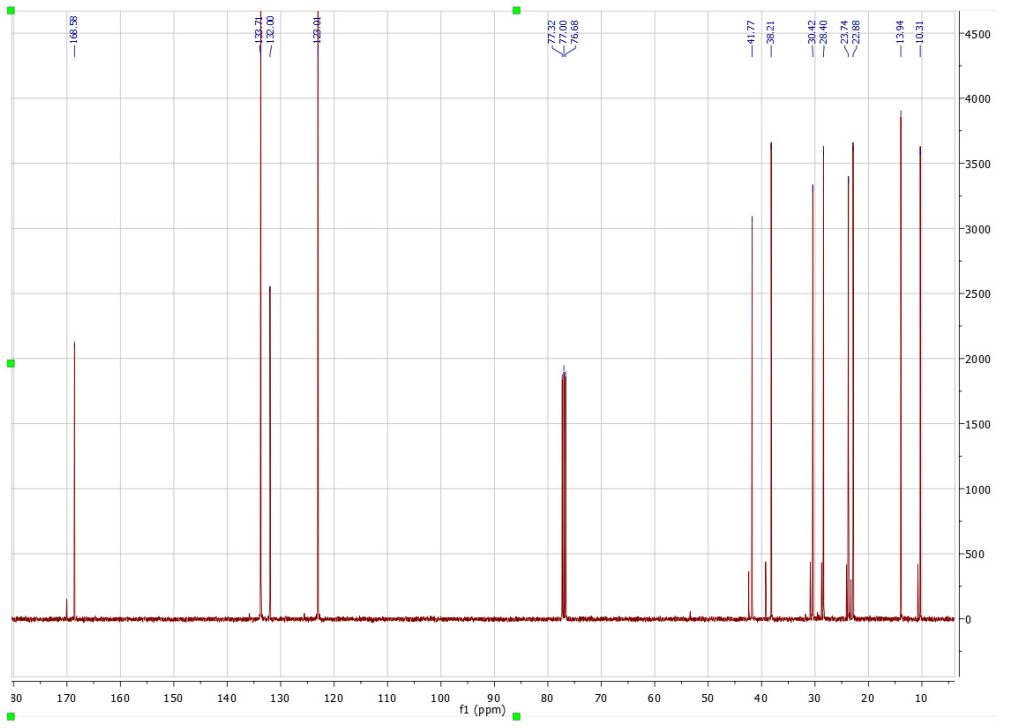
168.58
133.71
132.00
129.04
77.32
77.00
76.68
41.77
38.21
30.42
28.40
23.74
22.88
13.94
10.31
f1 (ppm)

1e

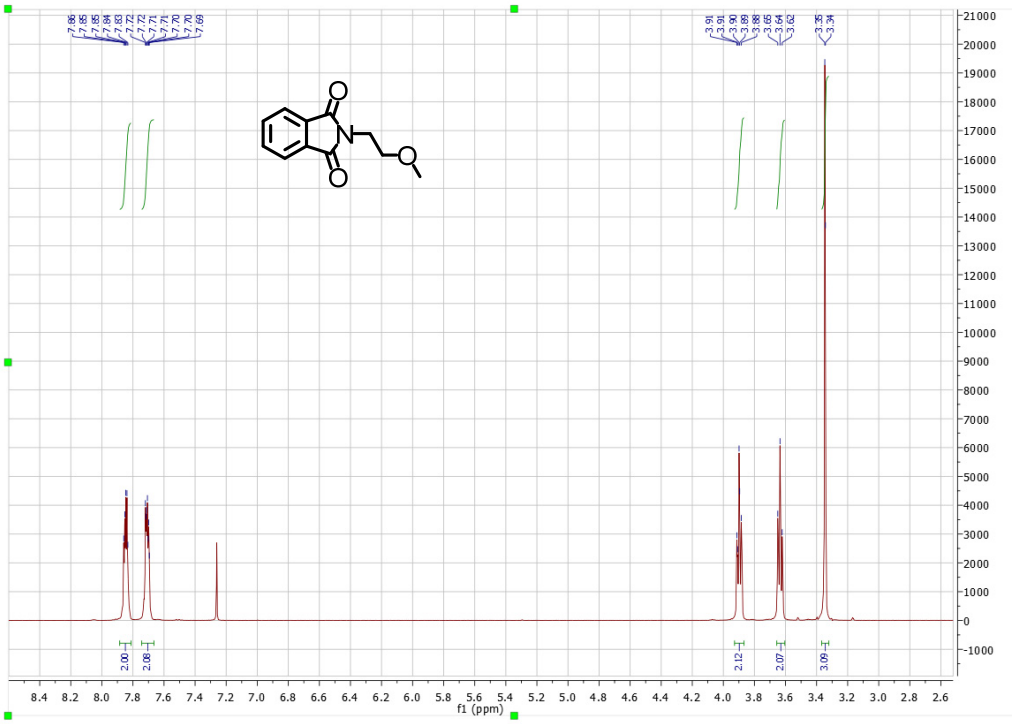
7.86
7.85
7.85
7.84
7.84
7.72
7.72
7.71
7.71
7.70
7.70
7.69
3.91
3.91
3.90
3.89
3.88
3.65
3.64
3.62
3.35
3.34
2.00
2.08
2.12
2.07
3.09
f1 (ppm)

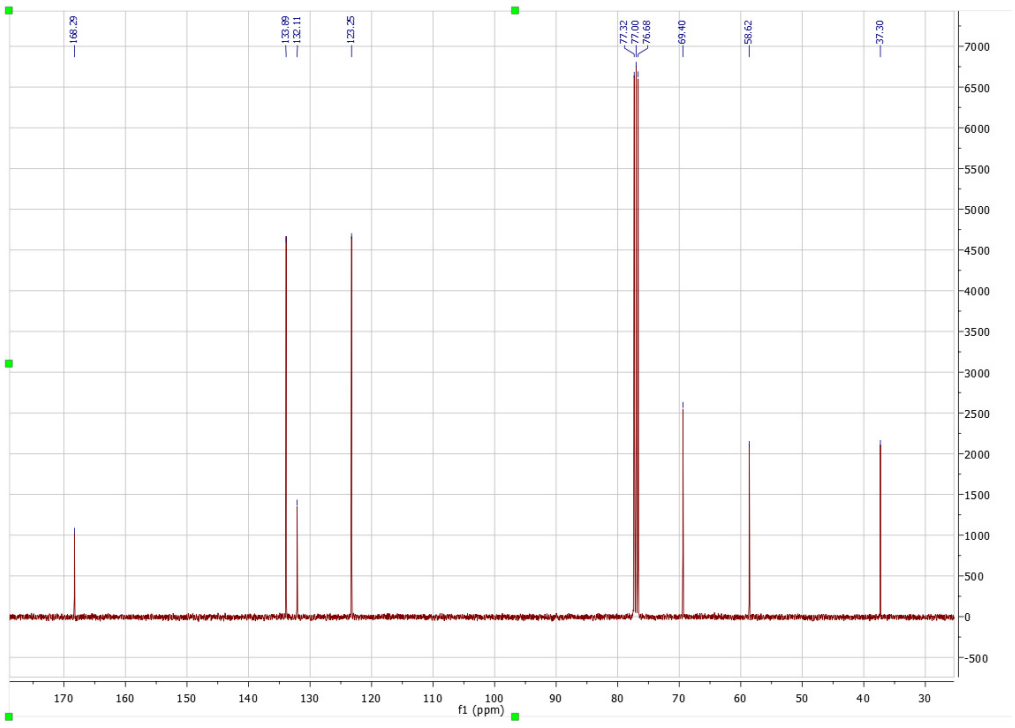
168.29
133.89
132.11
123.25
77.32
77.00
76.68
69.40
58.62
37.30
f1 (ppm)

1f

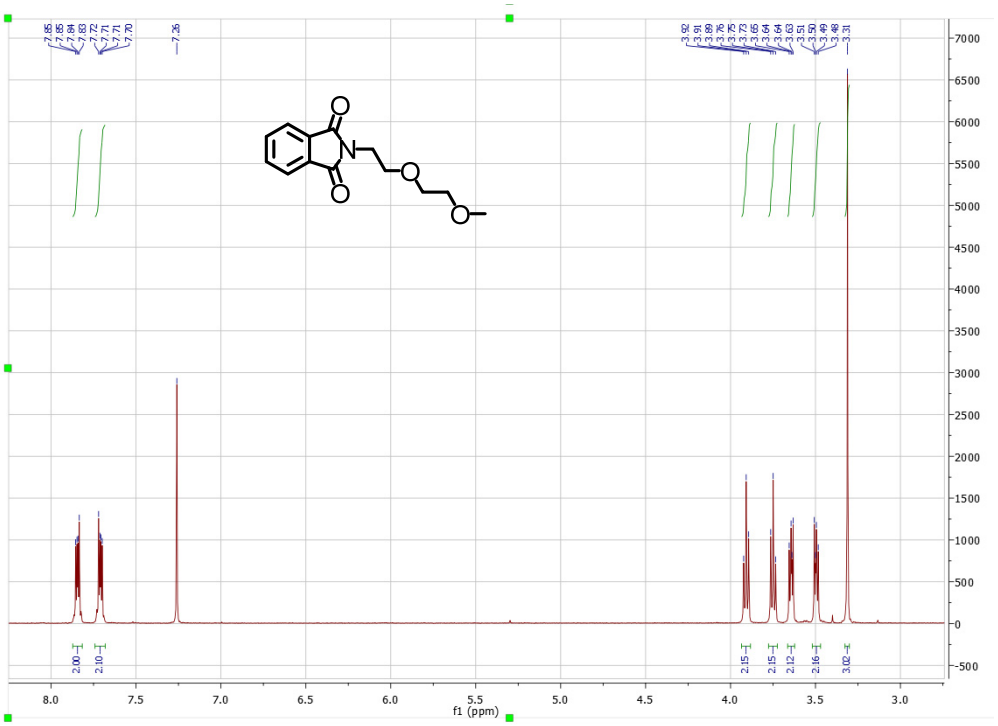
7.85
7.85
7.84
7.83
7.72
7.71
7.71
7.70
7.26
3.92
3.91
3.89
3.76
3.75
3.73
3.65
3.64
3.64
3.63
3.51
3.50
3.49
3.48
3.31
2.00
2.10
2.15
2.15
2.12
2.16
3.02
f1 (ppm)

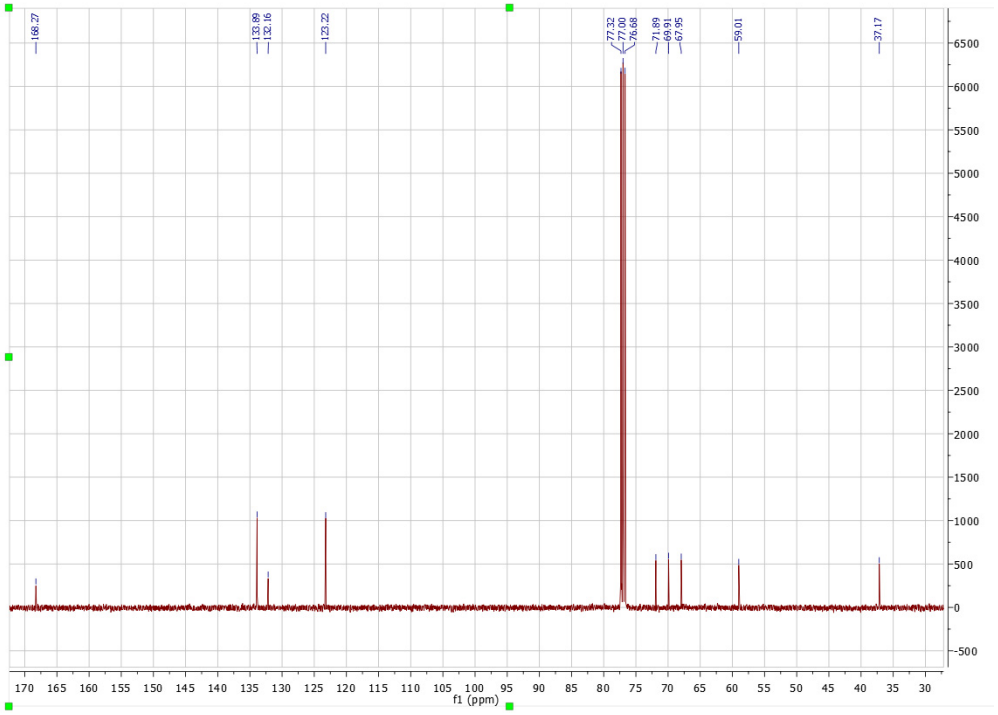
168.27
133.89
132.16
123.22
77.32
77.00
76.68
71.89
69.91
67.95
59.01
37.17
f1 (ppm)

1g

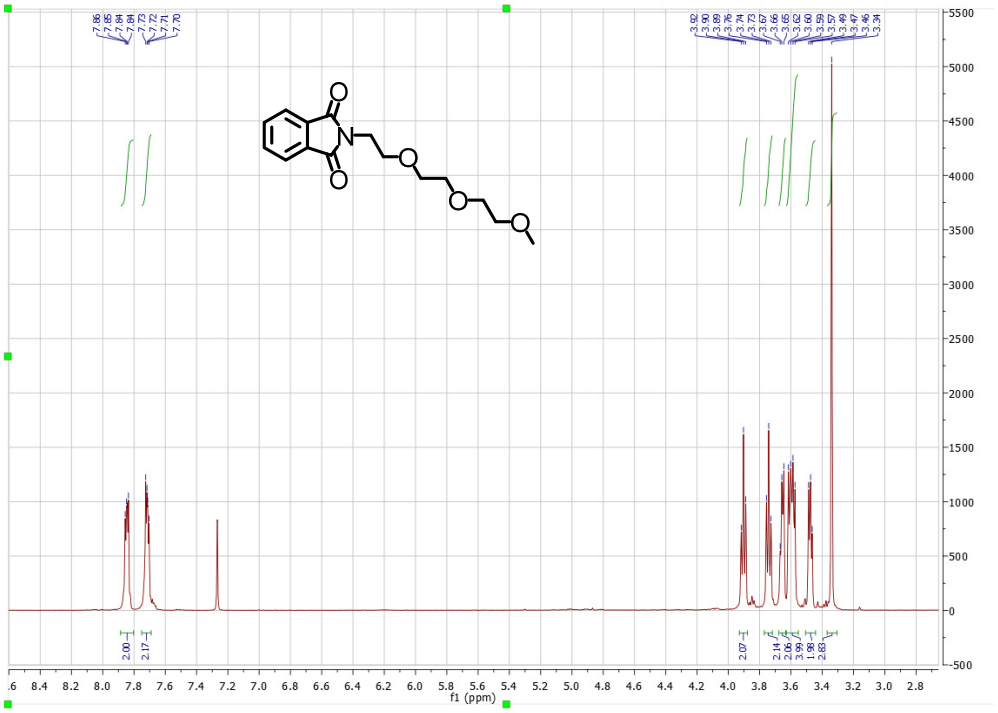
7.86
7.85
7.84
7.84
7.73
7.72
7.71
7.70
3.92
3.90
3.89
3.76
3.74
3.73
3.72
3.66
3.65
3.62
3.60
3.59
3.57
3.49
3.47
3.46
3.34
2.00
2.17
2.07
2.14
2.06
3.99
1.98
2.83
f1 (ppm)

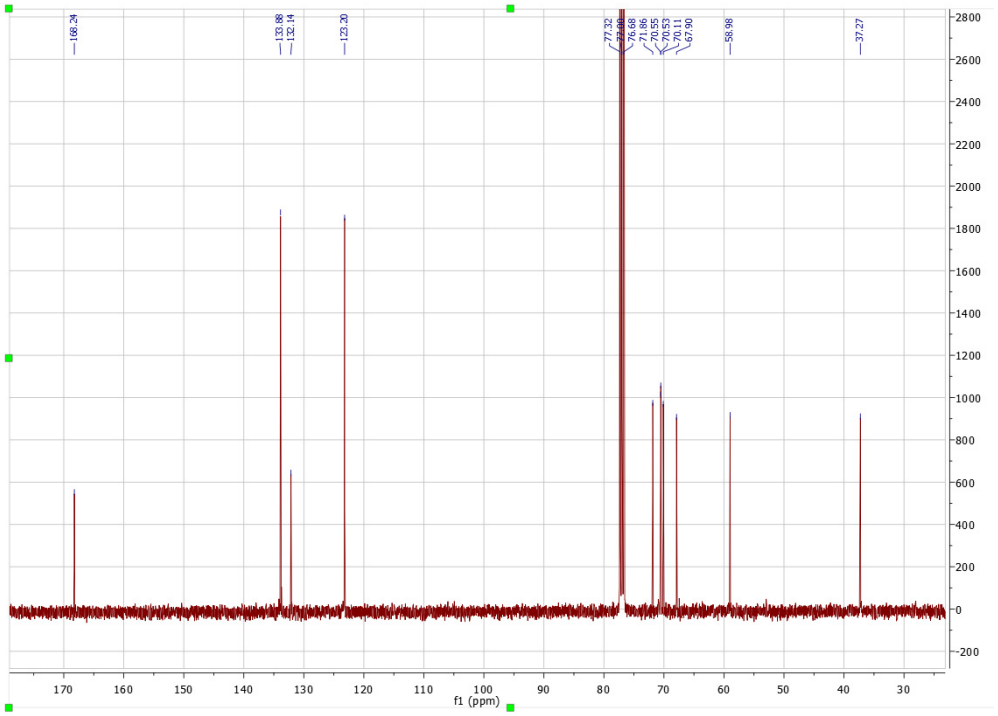
168.24
133.88
132.14
123.20
77.32
76.68
71.86
70.55
70.53
70.11
67.90
58.98
37.27
f1 (ppm)

2a

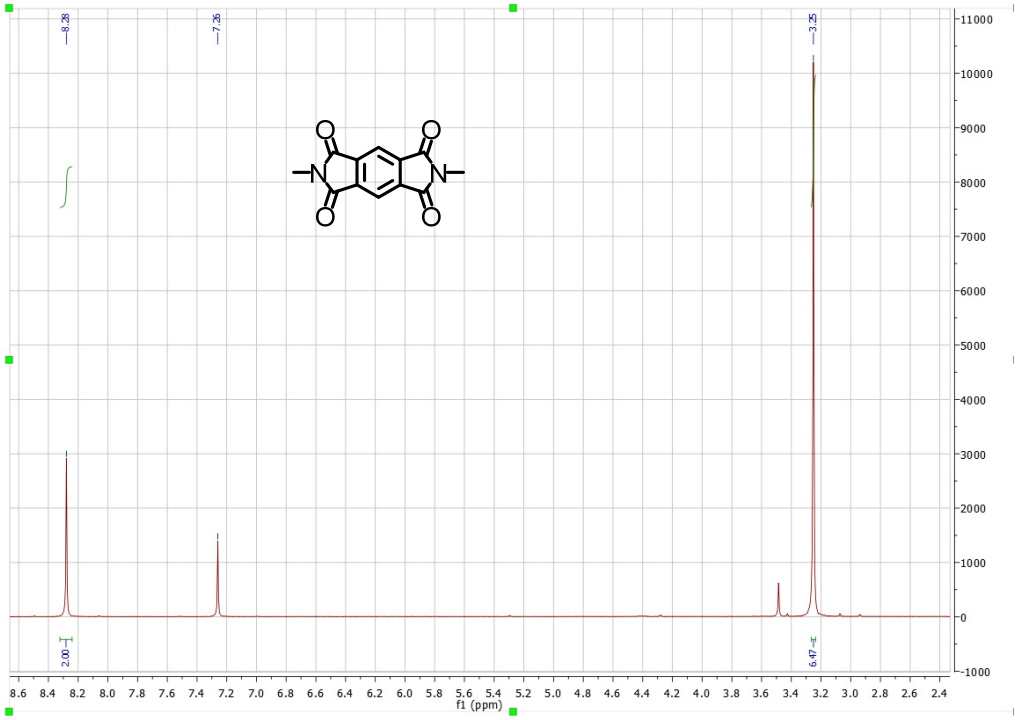
8.38
7.26
3.25
2.00
6.47
f1 (ppm)

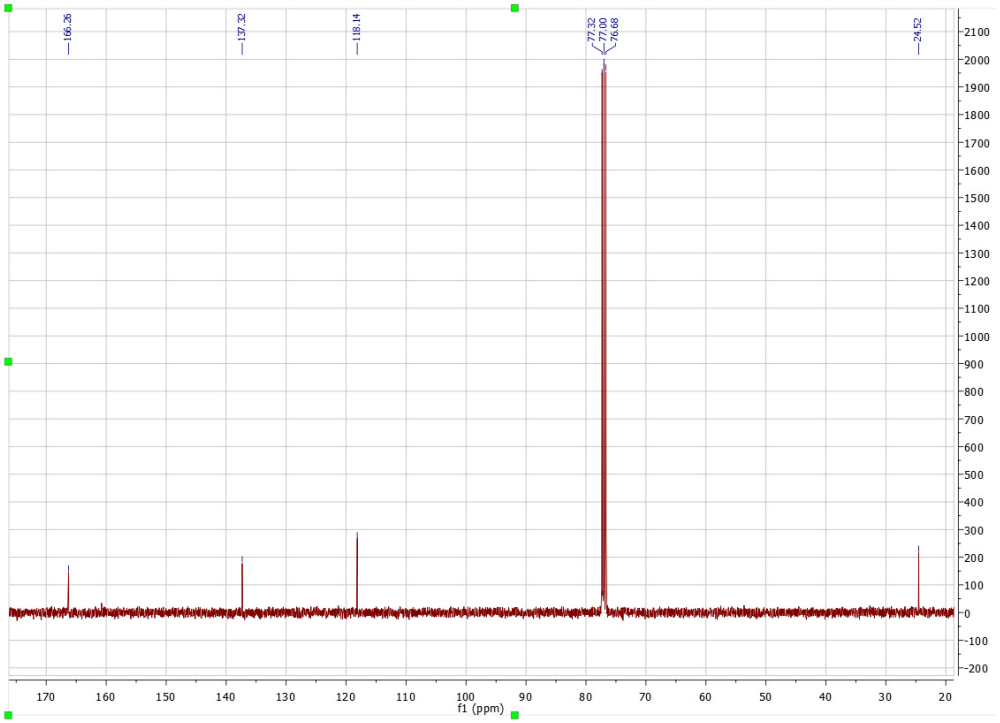
166.26
137.32
118.14
77.32
77.00
76.68
24.52
f1 (ppm)

2b

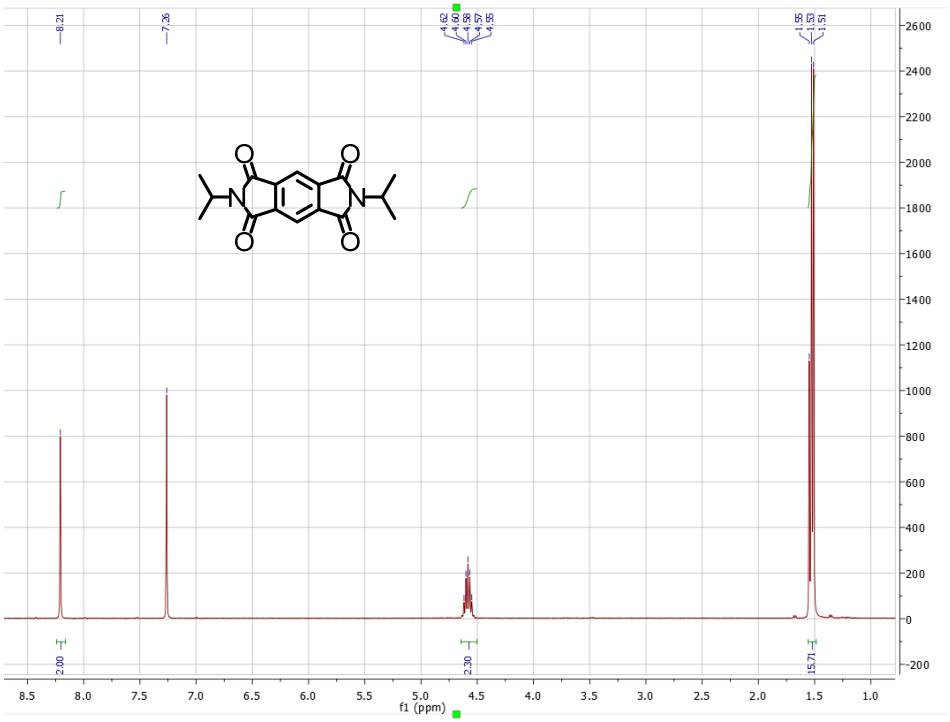
8.21
7.26
4.62
4.60
4.58
4.57
4.55
1.55
1.53
1.51
2.00
2.30
15.71
f1 (ppm)

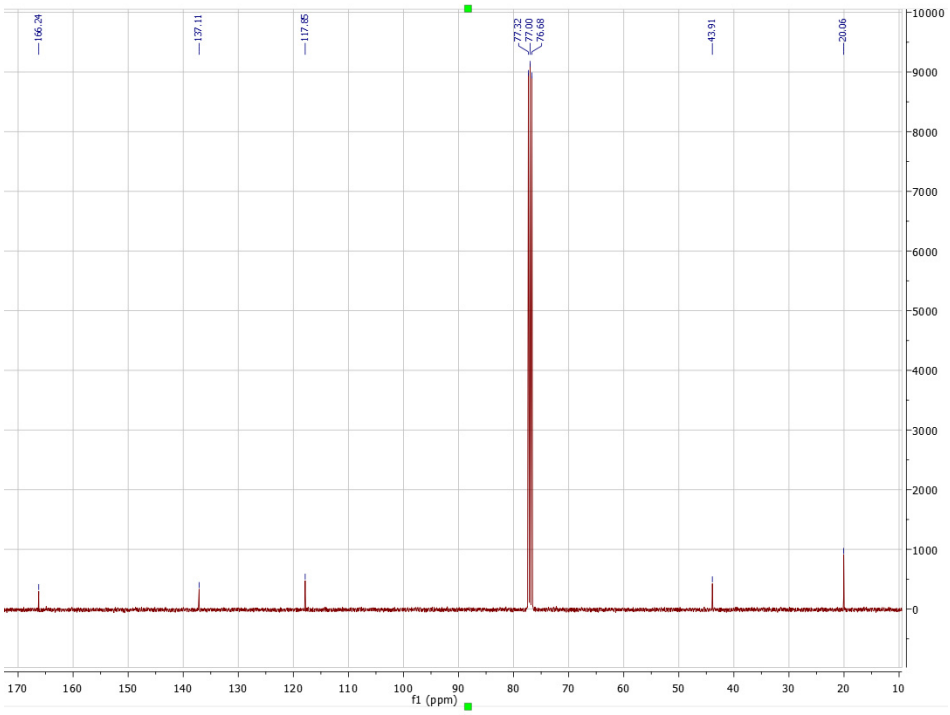
166.24
137.11
117.65
77.32
77.00
76.68
43.91
20.06
f1 (ppm)

2c

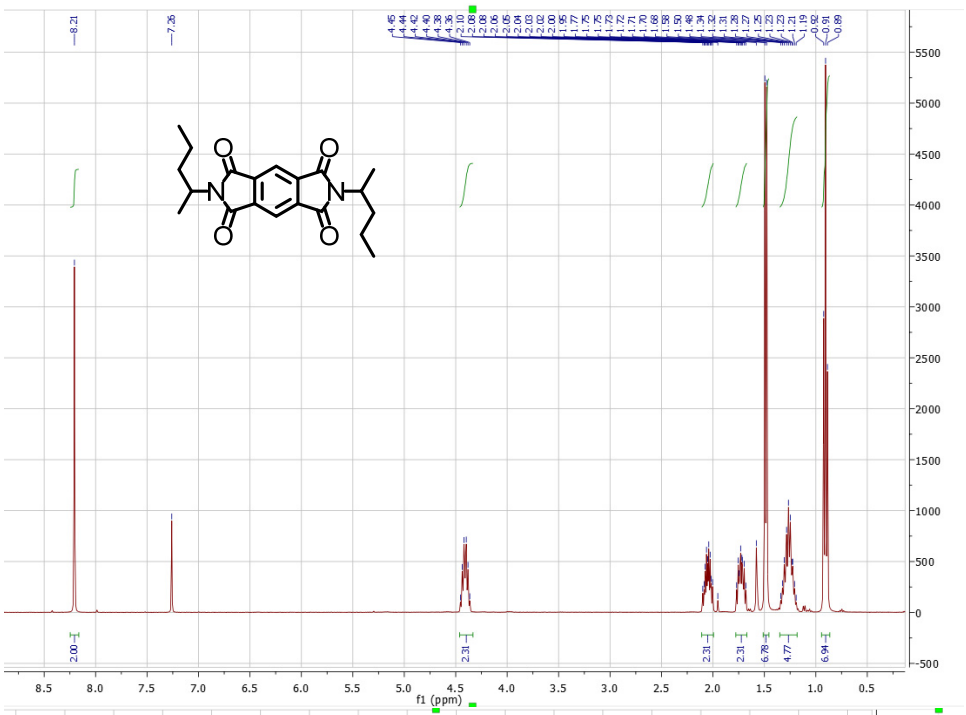

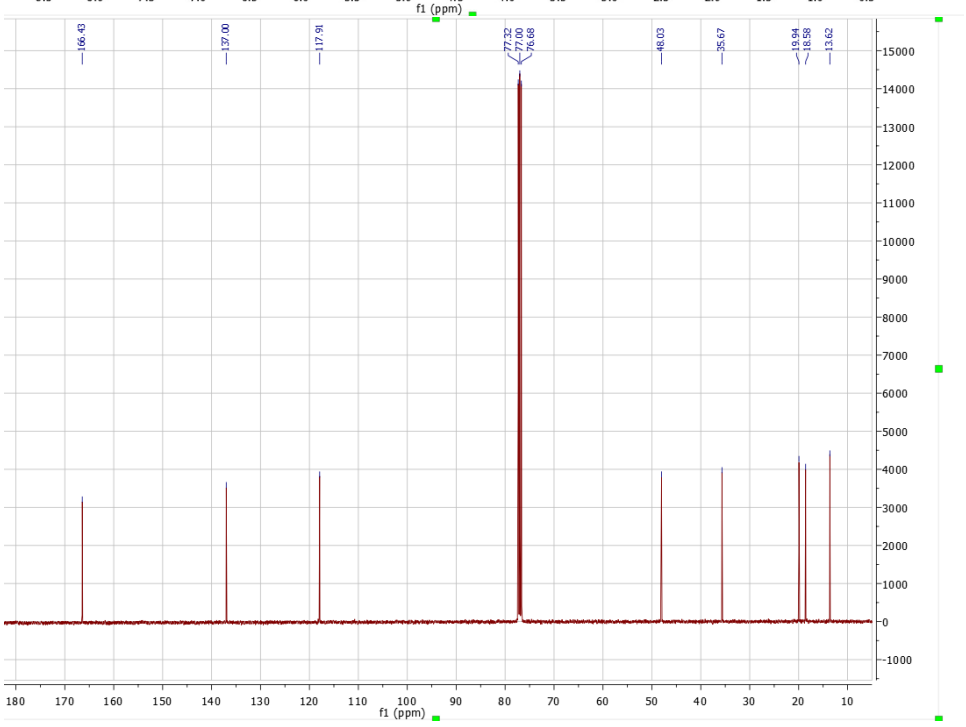

2d

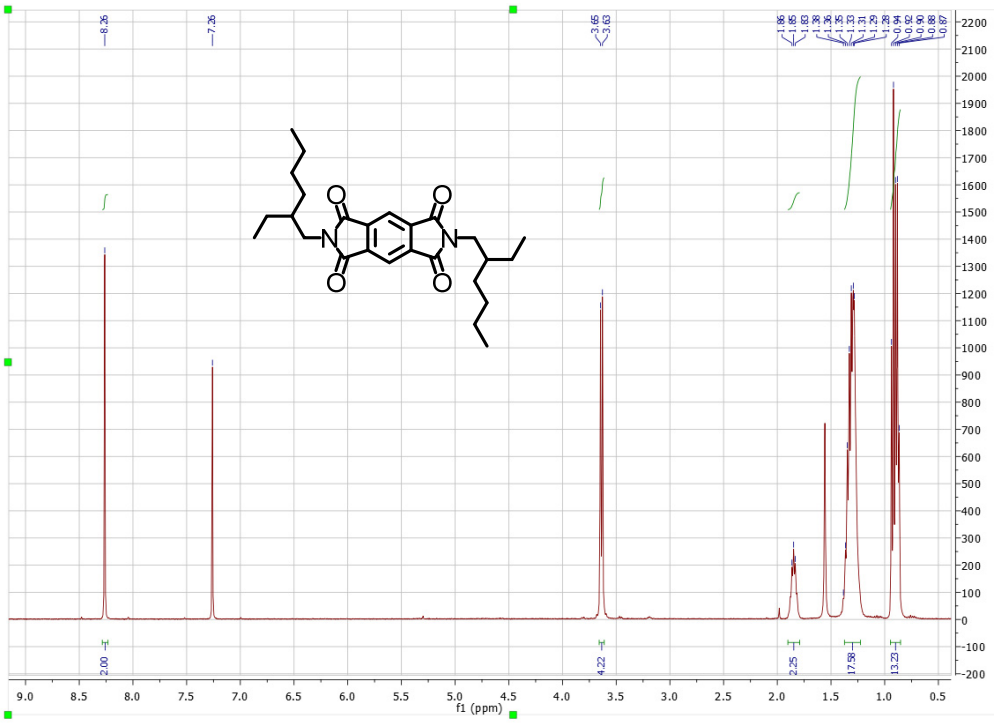
8.26
7.26
3.65
3.63
1.86
1.85
1.83
1.38
1.36
1.35
1.33
1.31
1.29
1.28
0.94
0.92
0.90
0.88
0.87
2.00
4.22
2.25
17.58
13.23
f1 (ppm)

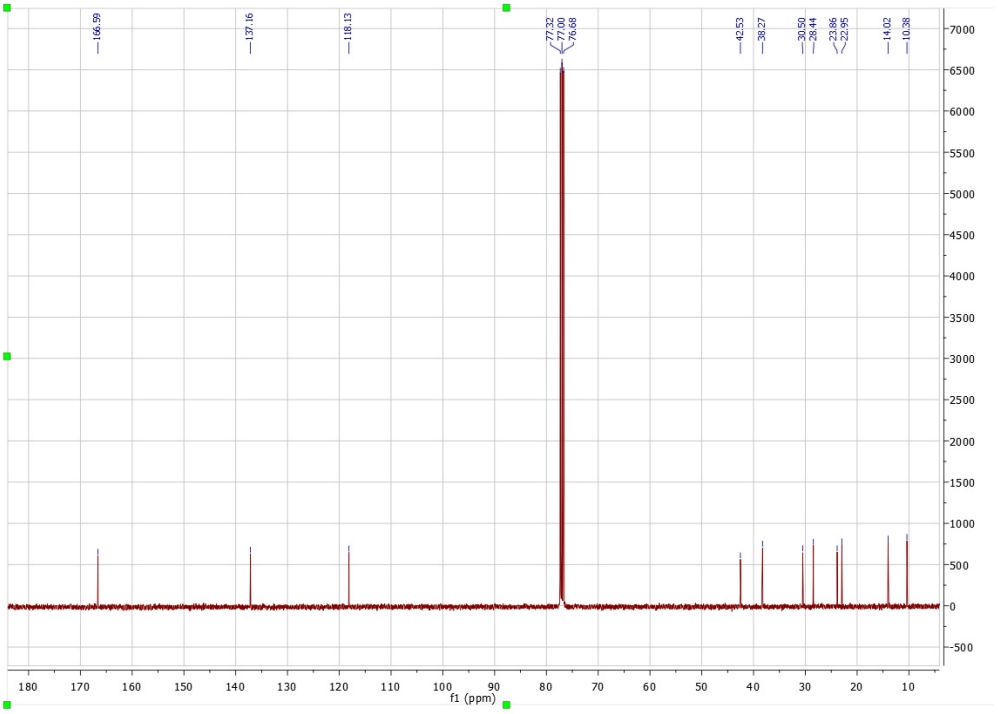
166.59
137.16
118.13
77.32
77.00
76.68
42.53
38.27
30.50
28.44
23.86
22.95
14.02
10.38
f1 (ppm)

2e

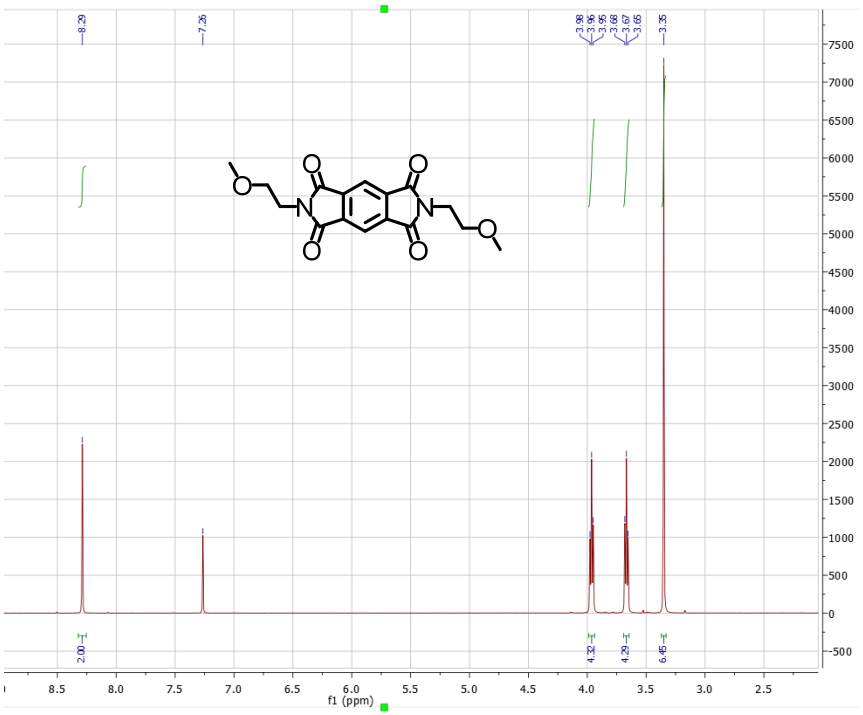
8.29
7.26
3.98
3.96
3.95
3.68
3.67
3.65
3.35
2.00
4.32
4.29
6.45
f1 (ppm)

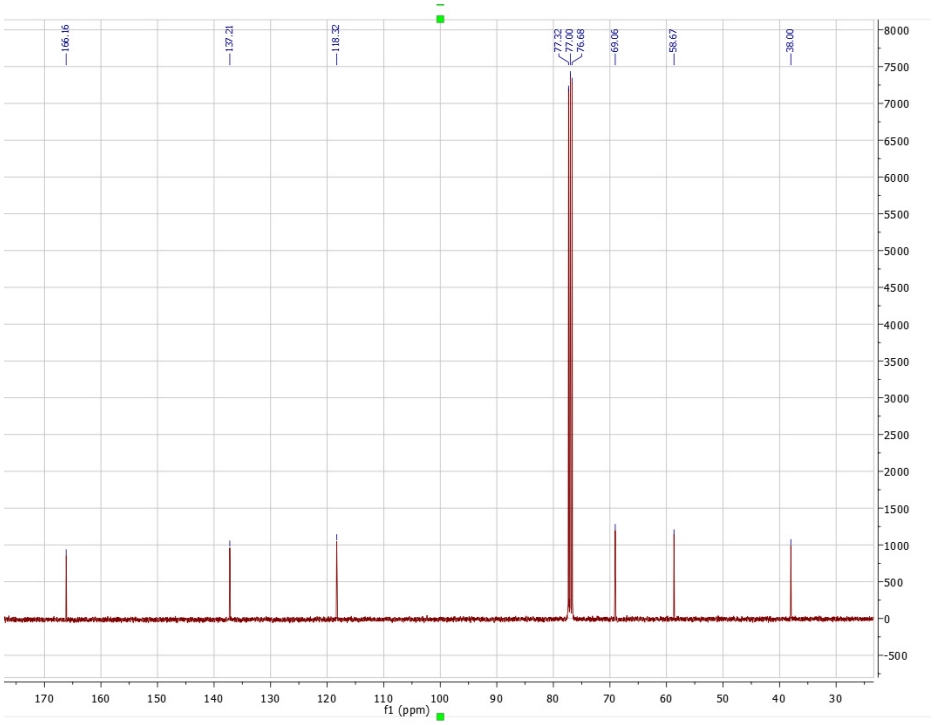
166.16
137.21
118.32
77.32
77.00
76.68
69.06
58.67
38.00
f1 (ppm)

2f

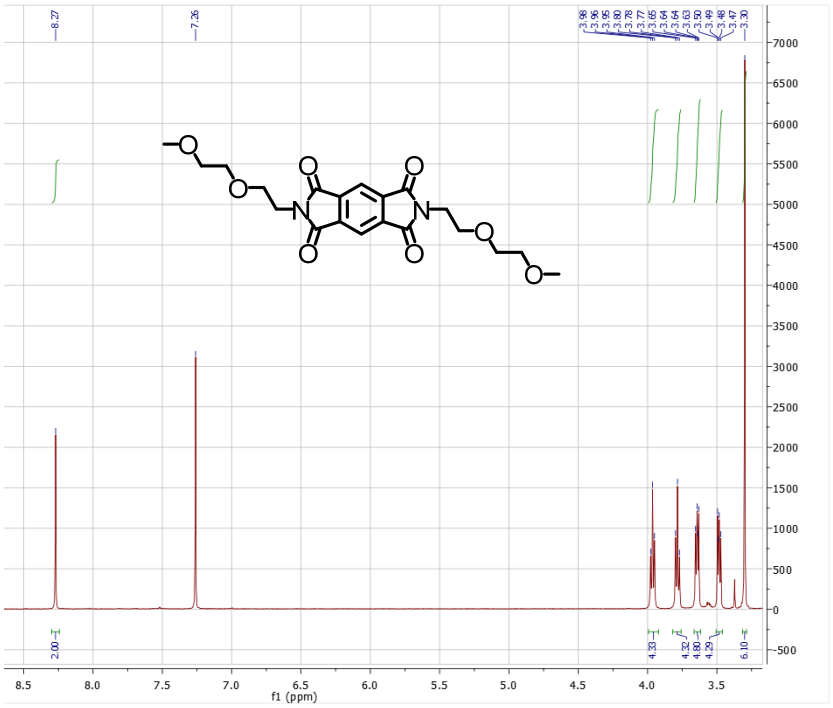
8.27
7.26
3.98
3.96
3.95
3.90
3.88
3.77
3.65
3.64
3.63
3.51
3.49
3.48
3.47
3.30
2.00
4.38
4.32
4.80
4.29
6.10
f1 (ppm)

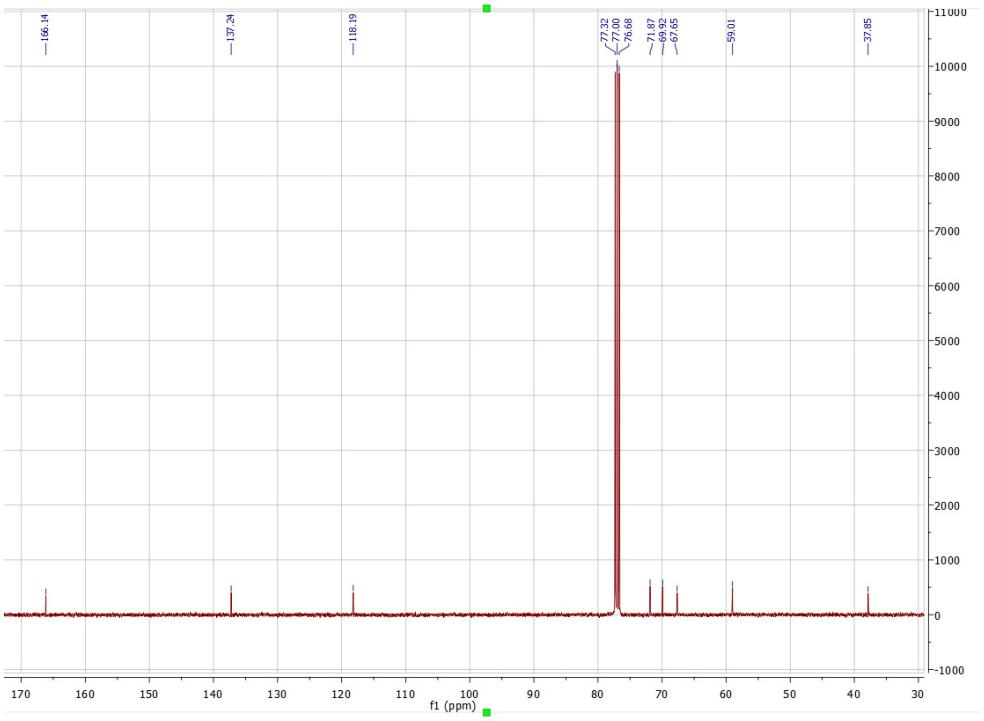
166.14
137.24
118.19
77.32
77.00
76.68
71.87
69.92
67.65
59.01
37.85
f1 (ppm)

2g

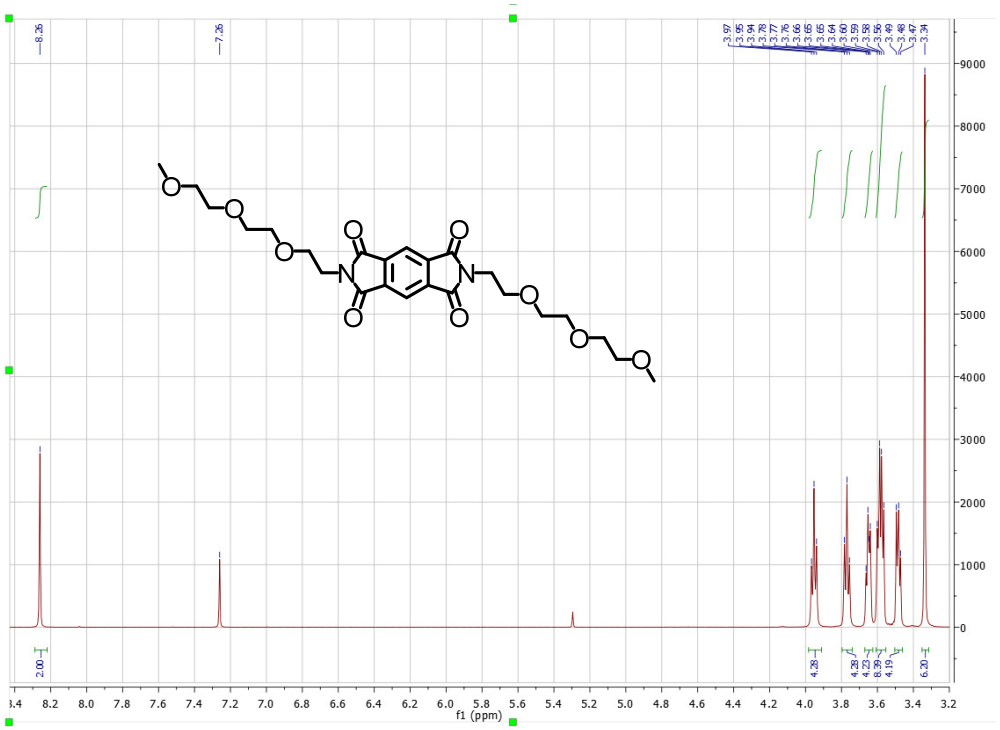
8.35
7.26
2.00
4.28
6.20
f1 (ppm)

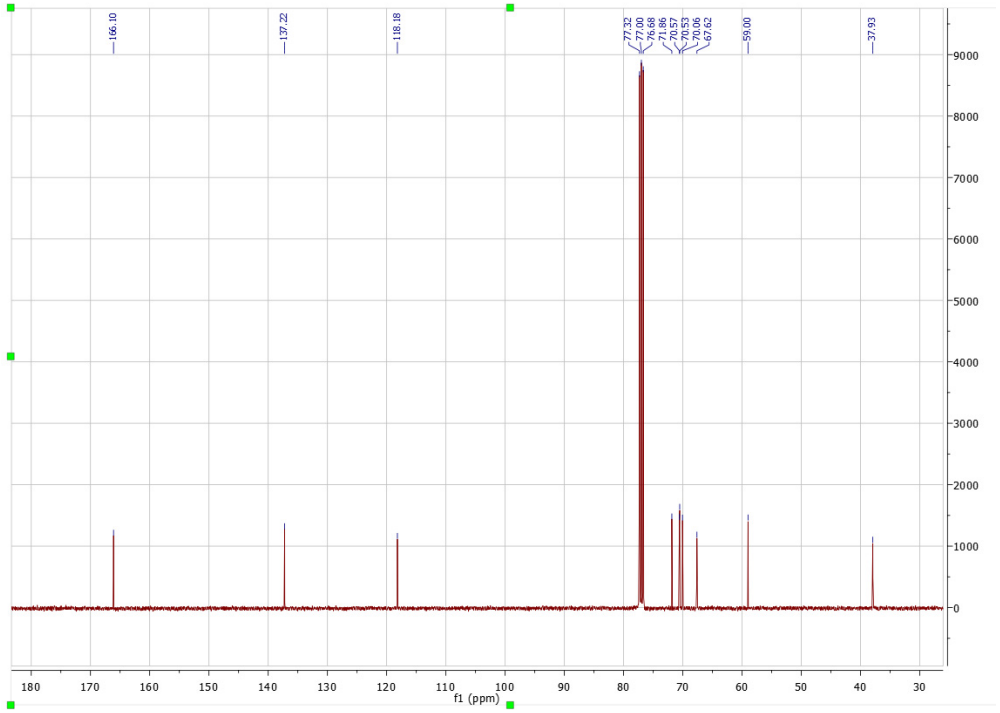
166.10
137.22
118.18
77.32
77.00
76.68
71.86
70.57
70.53
70.06
67.62
59.00
37.93
f1 (ppm)

2h

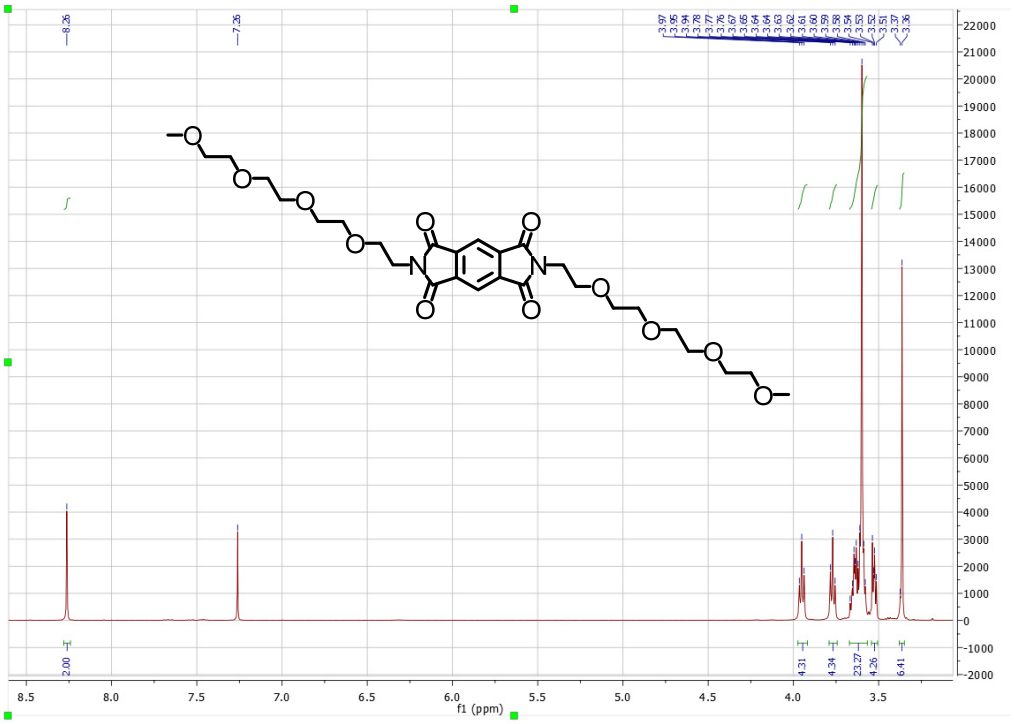
8.25
7.26
3.97
3.95
3.94
3.78
3.77
3.76
3.67
3.65
3.64
3.64
3.63
3.62
3.61
3.60
3.59
3.58
3.54
3.53
3.52
3.51
3.37
3.36
2.00
4.31
4.34
23.27
4.26
6.41
f1 (ppm)

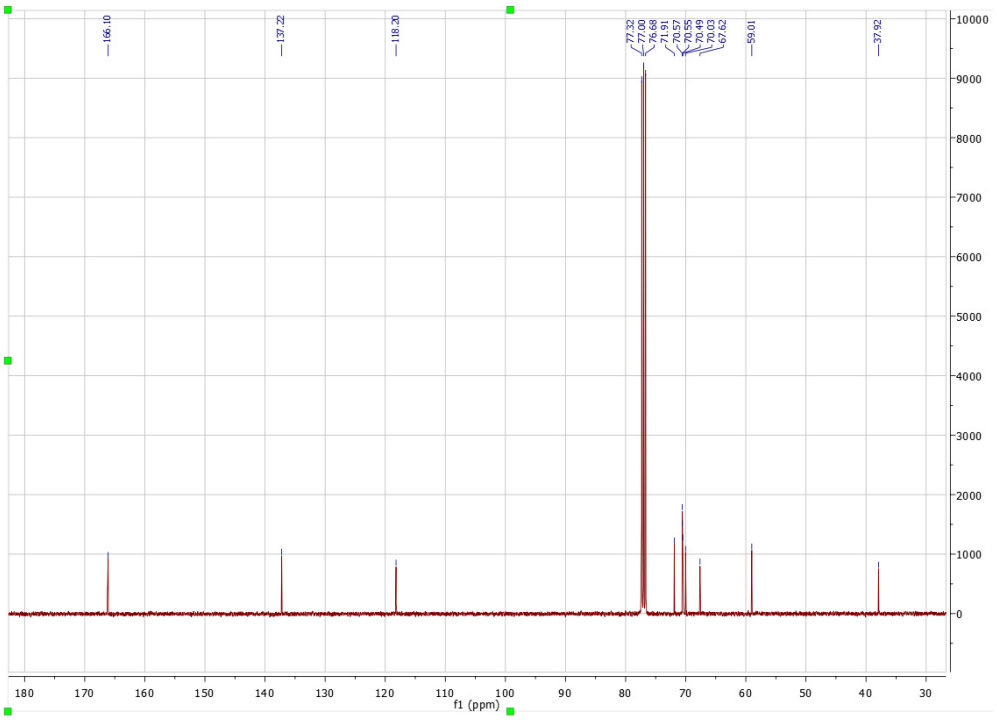
166.10
137.22
118.20
77.32
77.00
76.68
71.91
70.57
70.55
70.49
70.03
67.62
59.01
37.92
f1 (ppm)

2i

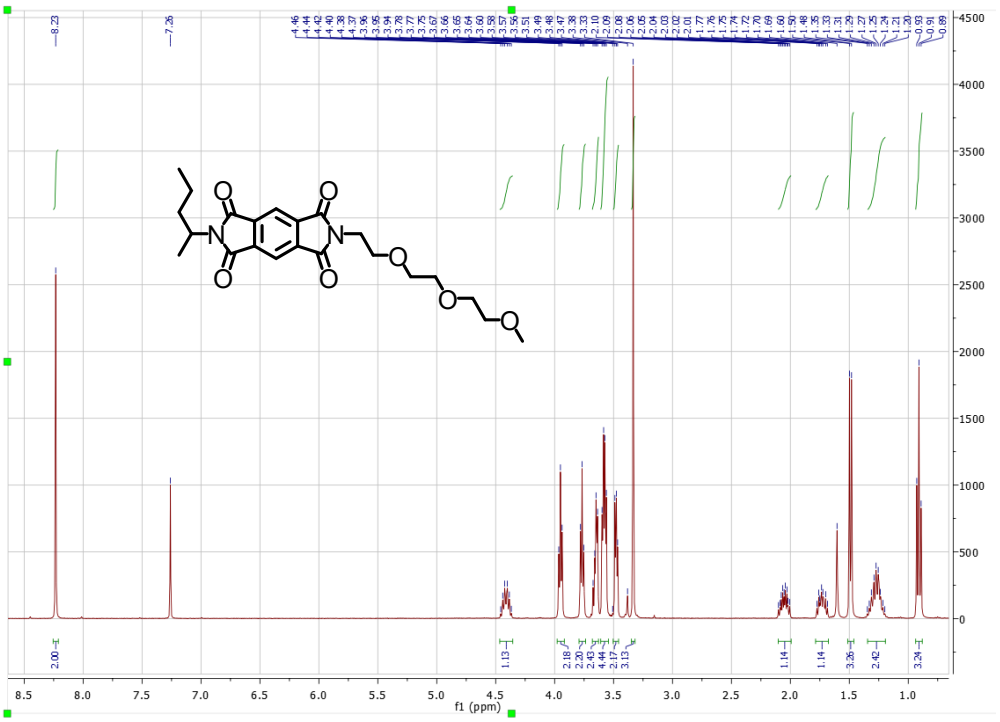
8.23
7.26
2.00
1.13
2.18
2.20
2.43
4.44
2.12
3.13
1.14
1.14
3.36
2.42
3.24
f1 (ppm)

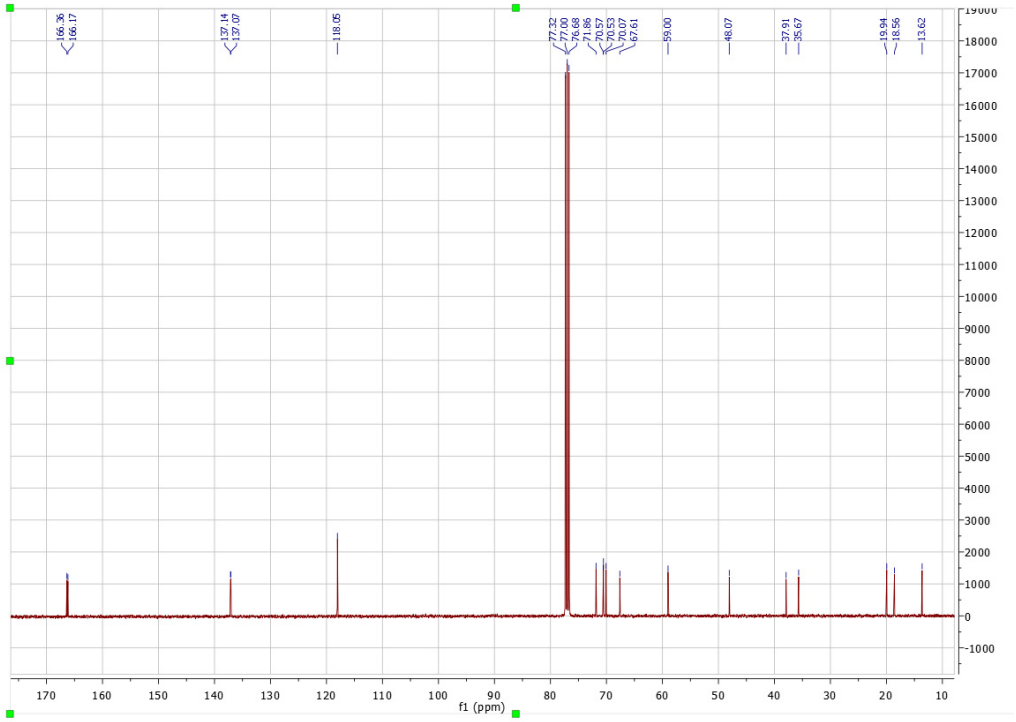
166.36
166.17
137.14
137.07
118.05
77.32
77.00
76.68
71.86
70.57
70.53
70.07
67.61
59.00
48.07
37.91
35.67
19.94
18.56
13.62
f1 (ppm)

3b

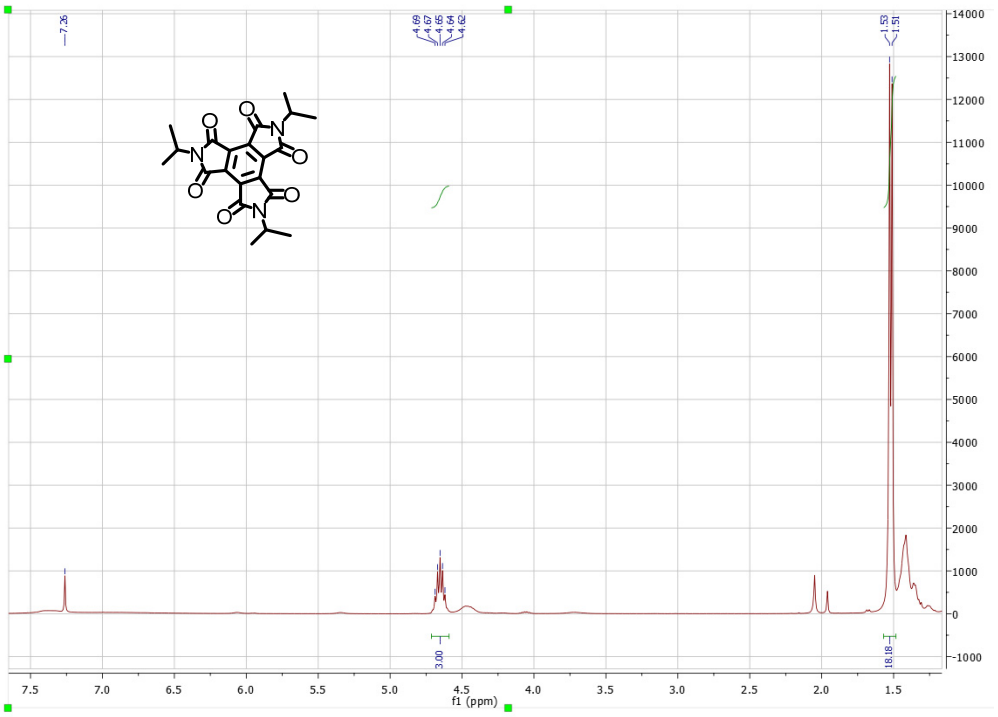
7.26
4.69
4.67
4.65
4.64
4.62
1.53
1.51
3.00
18.18
f1 (ppm)

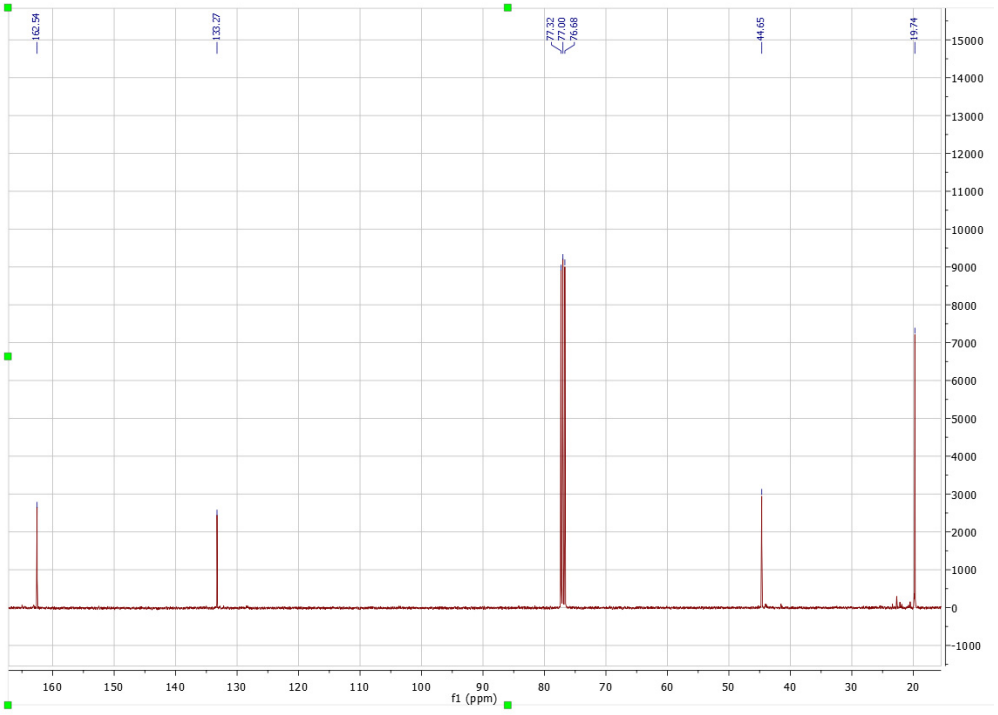
162.54
133.27
77.32
77.00
76.68
44.65
19.74
f1 (ppm)

3c

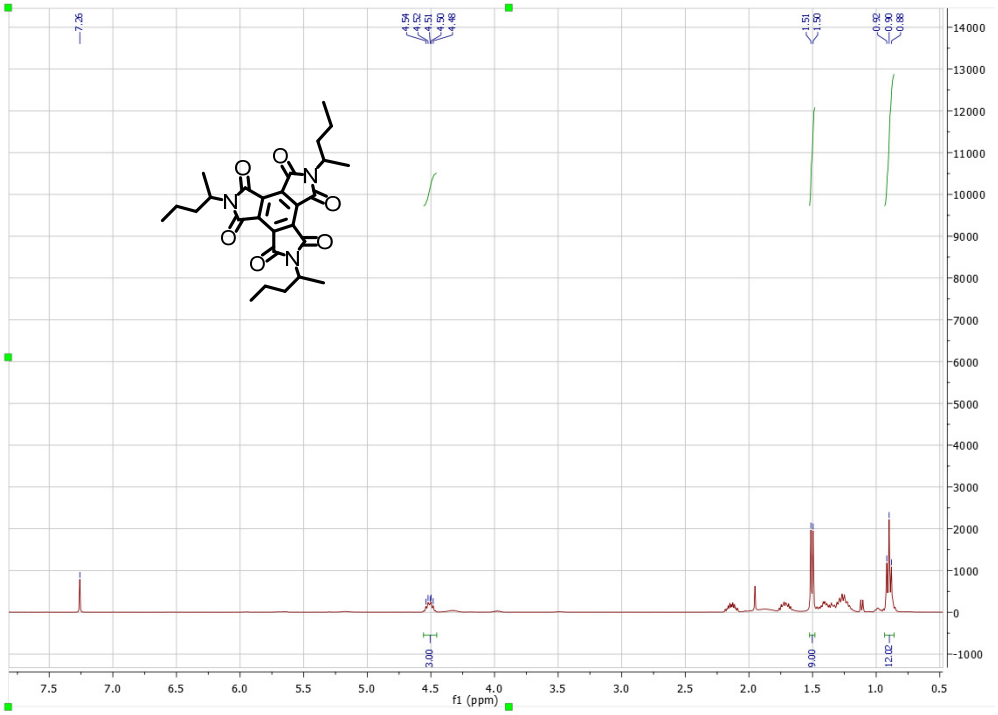
7.26
4.54
4.52
4.51
4.50
4.48
1.51
1.50
0.92
0.90
0.88
3.00
9.00
12.02
f1 (ppm)

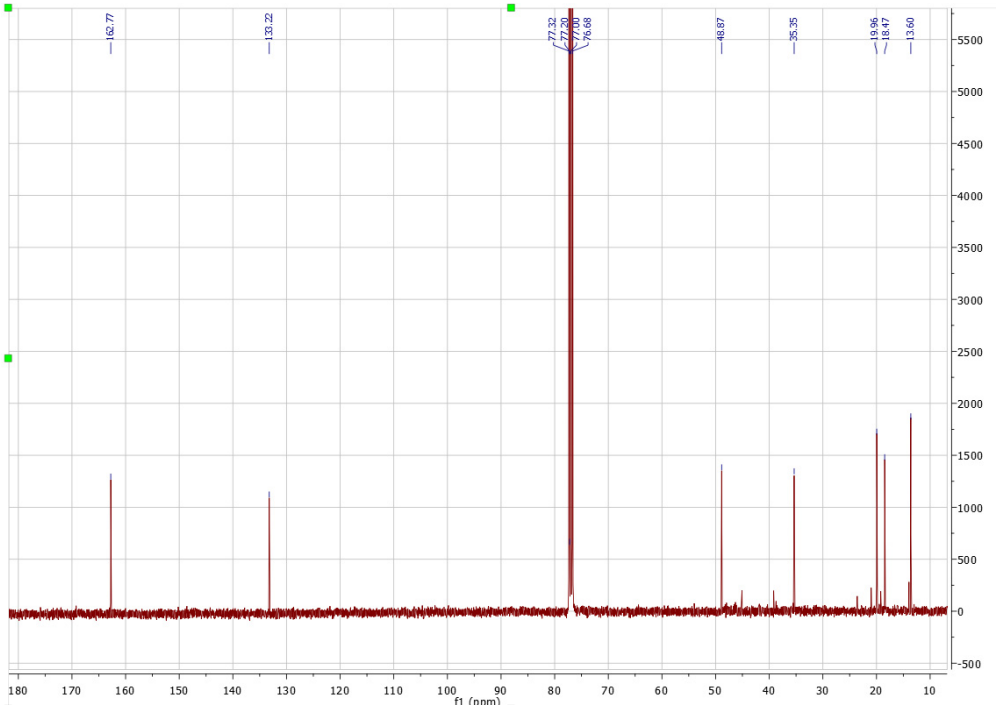
162.77
133.22
77.32
77.20
77.00
76.68
48.87
35.35
19.96
18.47
13.60
f1 (ppm)

3d

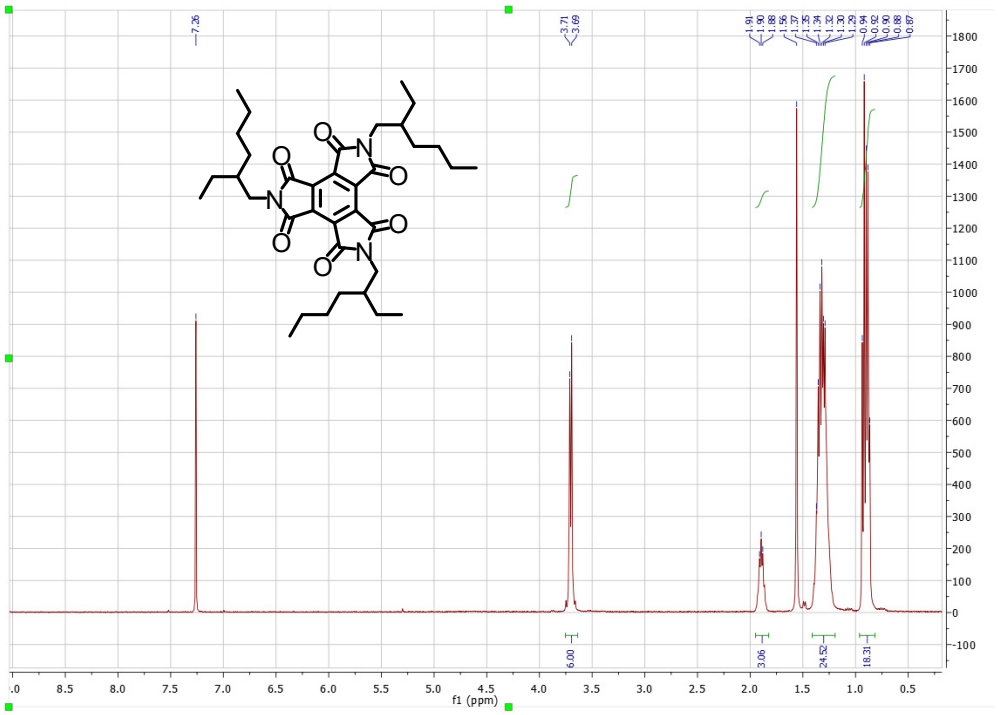
7.26
3.71
3.69
1.91
1.90
1.88
1.56
1.37
1.35
1.34
1.32
1.30
1.29
0.94
0.92
0.90
0.88
0.87
6.00
3.06
24.52
18.31
f1 (ppm)

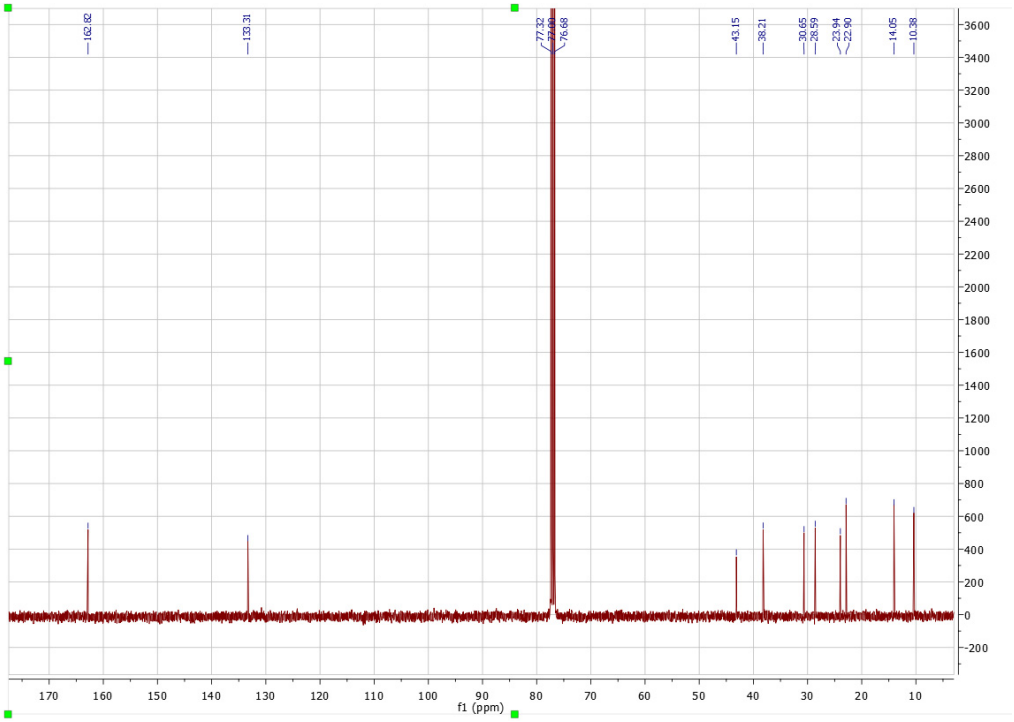
162.82
133.31
77.32
77.00
76.68
43.15
38.21
30.65
28.59
23.94
22.90
14.05
10.38
f1 (ppm)

3e

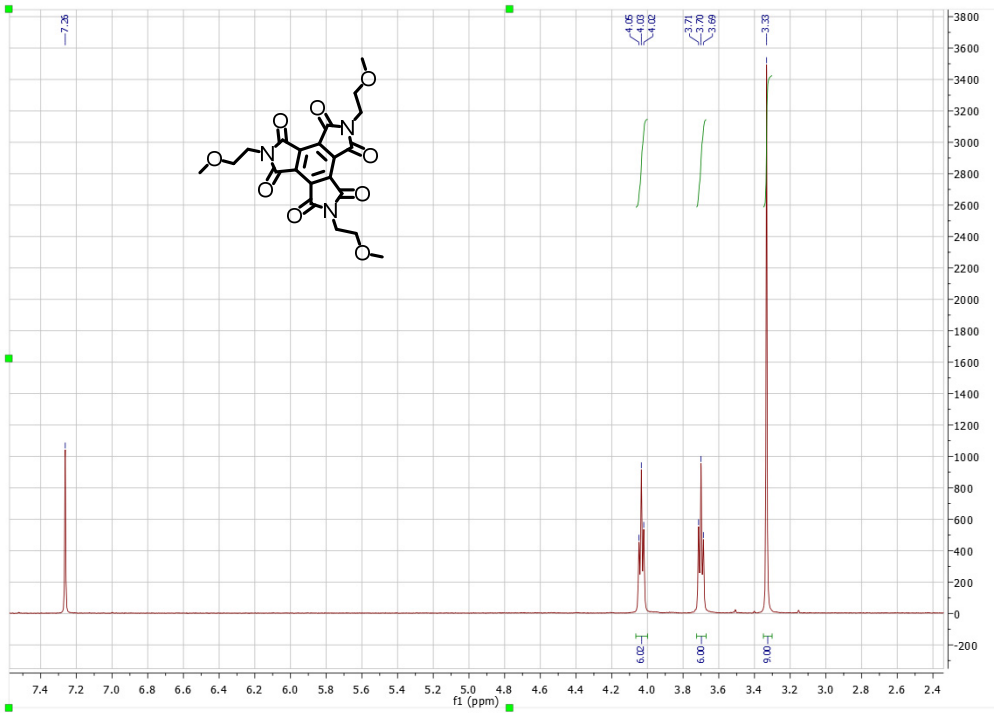
7.26
4.05
4.03
4.02
3.71
3.70
3.69
3.33
6.02
6.00
9.00
f1 (ppm)

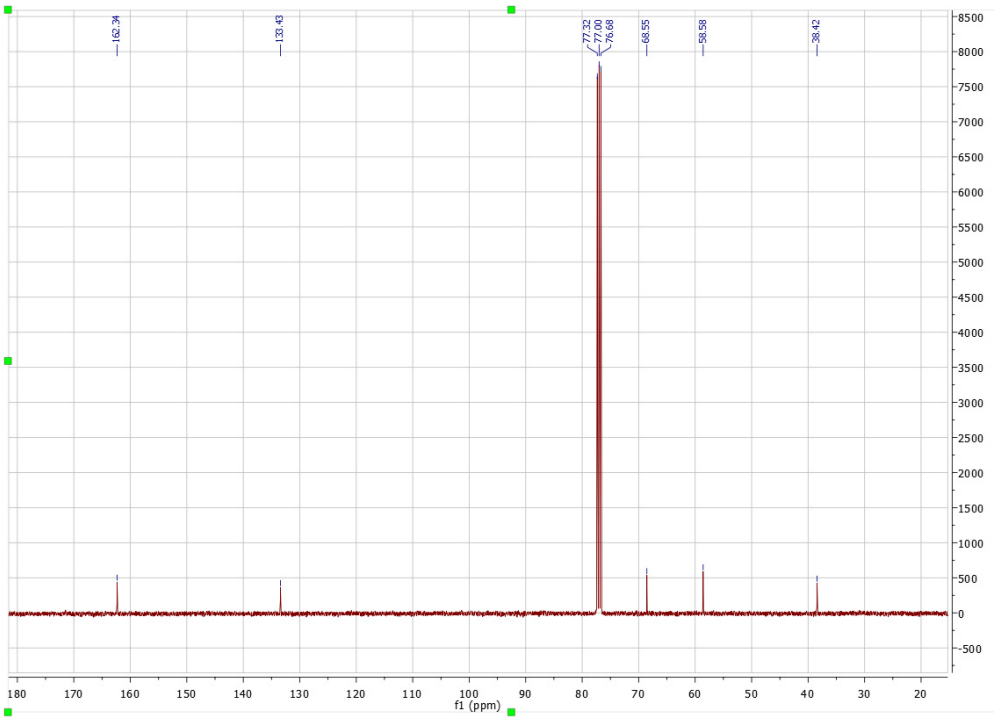
162.34
133.43
77.32
77.00
76.68
68.55
58.58
38.42
f1 (ppm)

3f

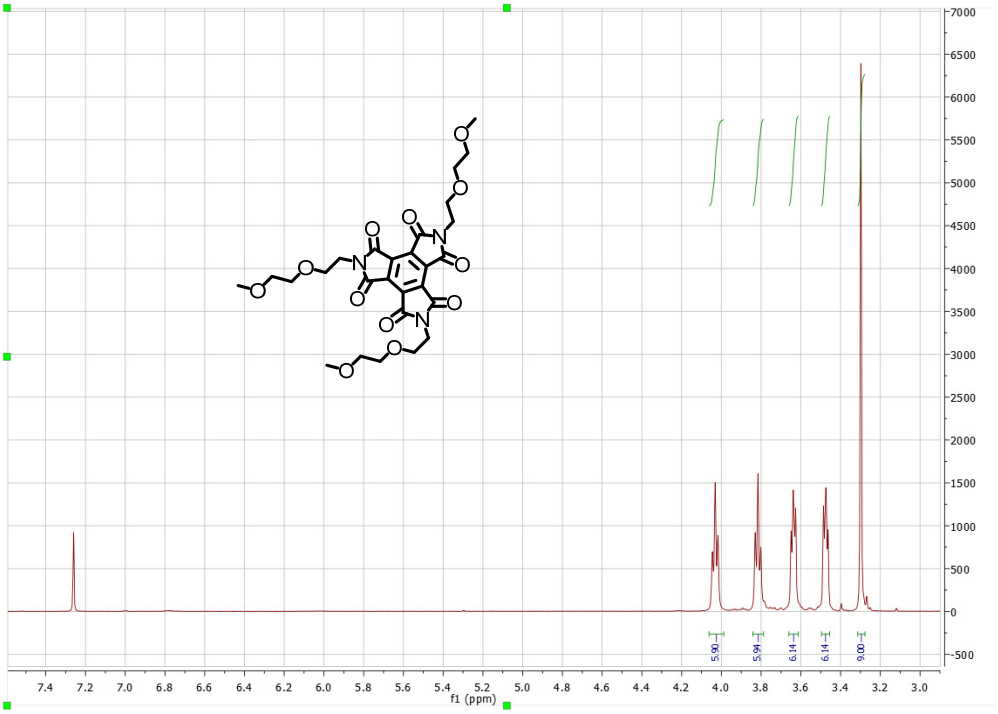
5.00
5.04
6.14
6.14
9.00
f1 (ppm)

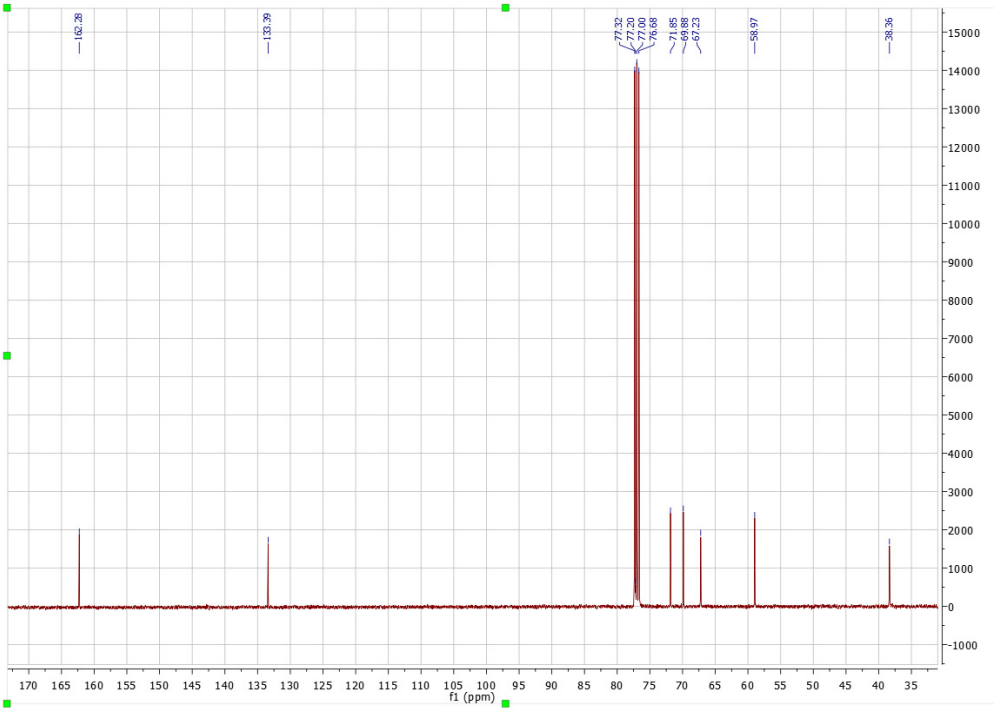
162.28
133.39
77.32
77.20
77.00
76.68
71.85
69.88
67.23
58.97
38.36
f1 (ppm)

3g

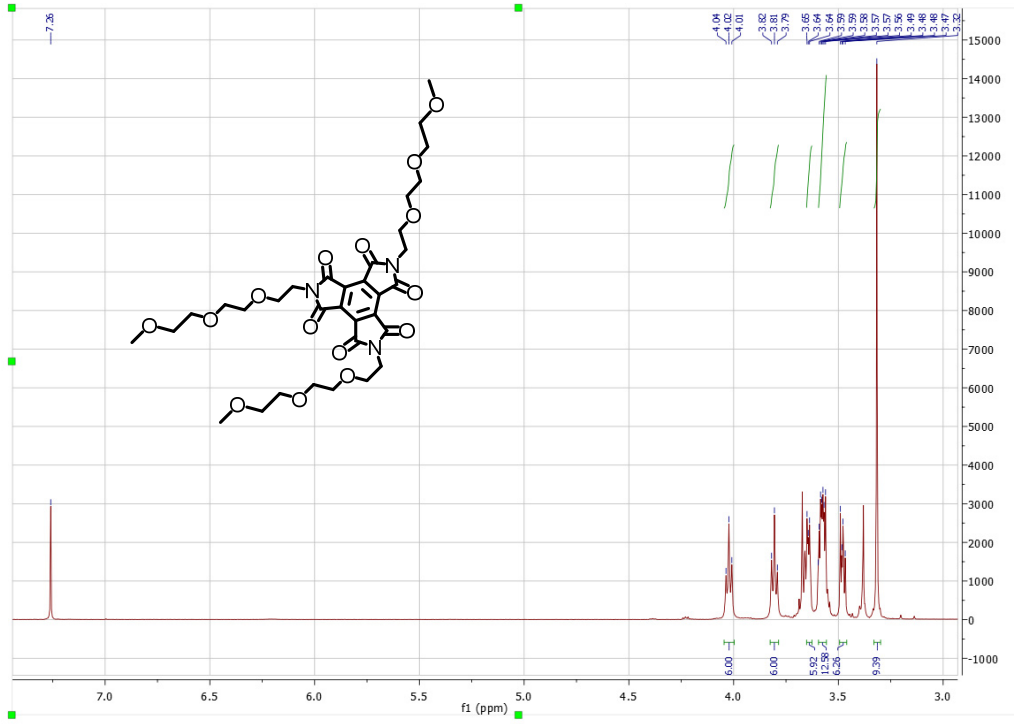
7.26
4.04
4.02
4.01
3.82
3.81
3.79
3.65
3.64
3.64
3.59
3.59
3.58
3.57
3.57
3.56
3.49
3.48
3.48
3.47
3.32
6.00
6.00
5.92
12.38
6.26
9.39
f1 (ppm)

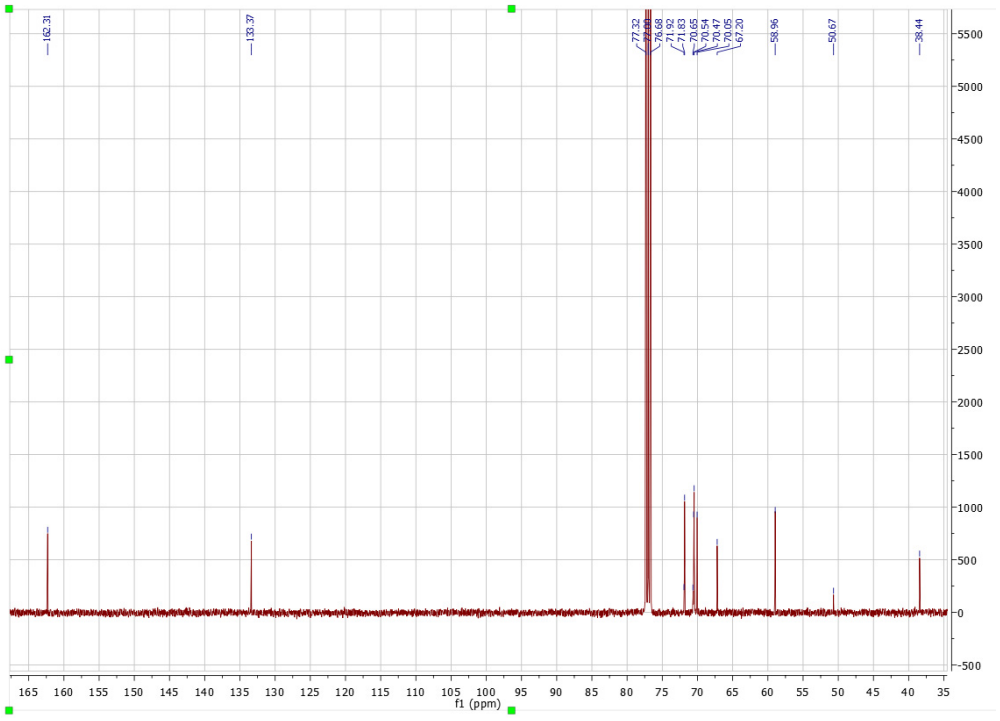
162.31
133.37
77.32
76.68
71.92
71.83
70.65
70.54
70.47
70.05
67.20
58.96
50.67
38.44
f1 (ppm)

3h

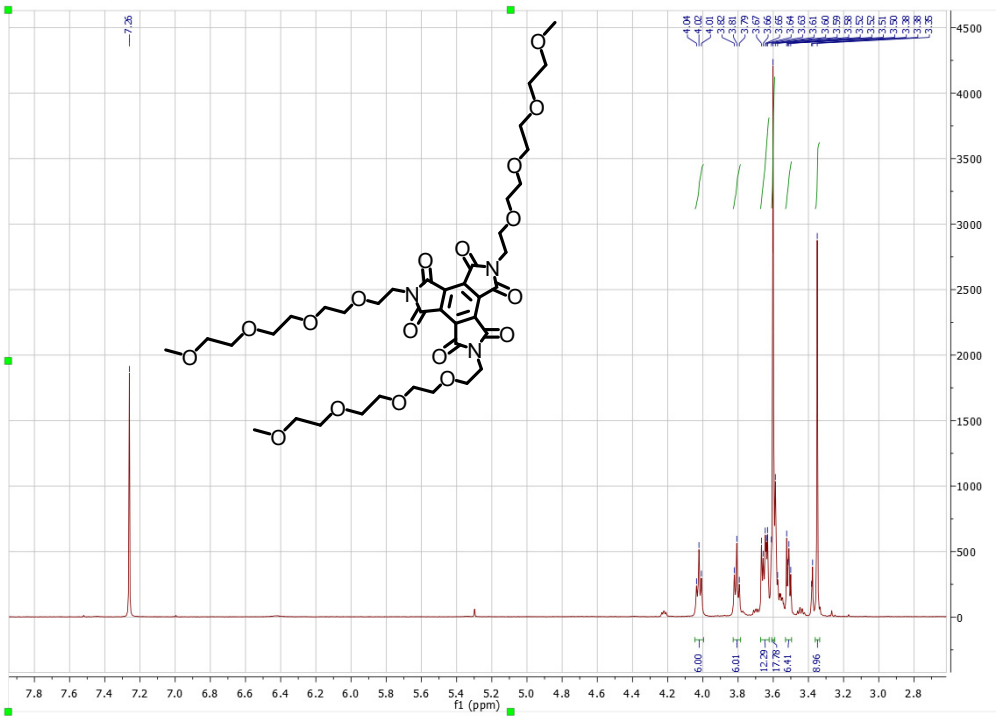
7.26
4.04
4.02
4.01
3.82
3.81
3.79
3.67
3.66
3.65
3.64
3.63
3.61
3.60
3.59
3.58
3.52
3.52
3.51
3.50
3.38
3.38
3.35
6.00
6.01
12.29
17.78
6.41
8.96
f1 (ppm)

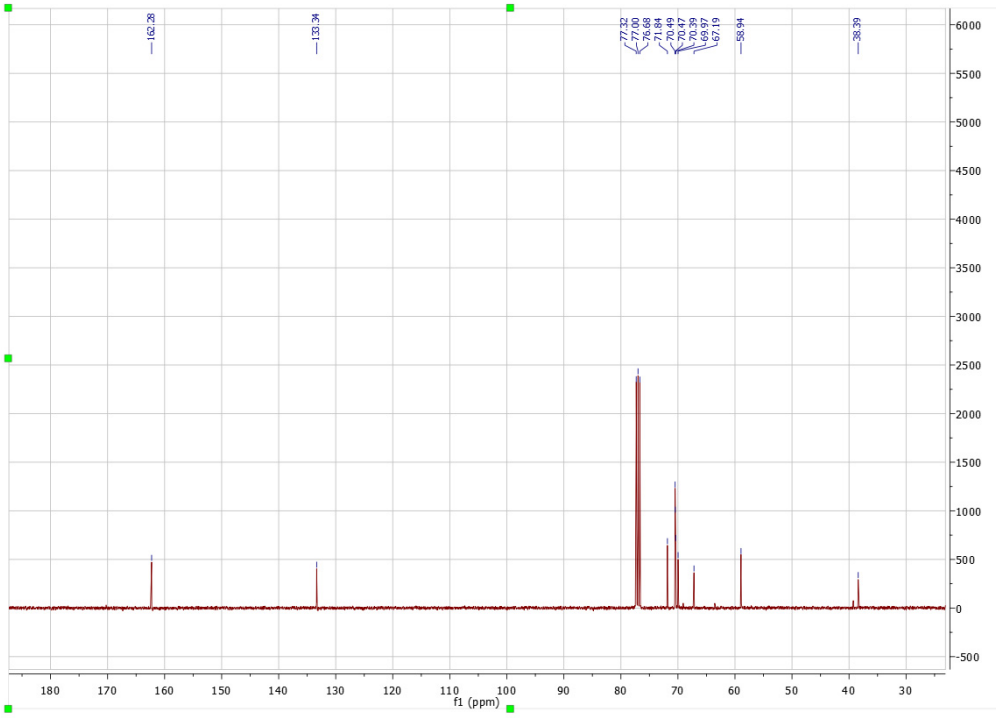
162.28
133.34
77.32
77.00
76.68
71.84
70.49
70.47
70.39
69.97
67.19
58.94
38.39
f1 (ppm)

References

(1) Wang, Y.; Zhou, Y.; Lei, M.; Hou, J.; Jin, Q.; Guo, D.; Wu, W. PPh_3/I_2/HCOOH: An Efficient CO Source for the Synthesis of Phthalimides. *Tetrahedron* **2019**, *75* (9), 1180–1185. https://doi.org/10.1016/j.tet.2019.01.023.

(2) Wu, X.-F.; Oschatz, S.; Sharif, M.; Flader, A.; Krey, L.; Beller, M.; Langer, P. Palladium-Catalyzed Carbonylative Synthesis of Phthalimides from 1,2-Dibromoarenes with Molybdenum Hexacarbonyl as Carbon Monoxide Source. *Adv. Synth. Catal.* **2013**, *355* (18), 3581–3585. https://doi.org/10.1002/adsc.201300585.

(3) Khedkar, M. V.; Shinde, A. R.; Sasaki, T.; Bhanage, B. M. Immobilized Palladium Metal Containing Ionic Liquid Catalyzed One Step Synthesis of Isoindole-1,3-Diones by Carbonylative Cyclization Reaction. *J. Mol. Catal. Chem.* **2014**, *385*, 91–97. https://doi.org/10.1016/j.molcata.2014.01.018.

(4) Sudarga Tjakraatmadja, A. A. J.; Lüdtke, C.; Kulak, N. Tuning the DNA Binding and Cleavage of Bpa Cu(II) Complexes by Ether Tethers with Hydroxyl and Methoxy Groups. *Inorganica Chim. Acta* **2016**, *452*, 159–169. https://doi.org/10.1016/j.ica.2016.02.034.

(5) Zhang, Y.; Yin, Q.; Yen, J.; Li, J.; Ying, H.; Wang, H.; Hua, Y.; Chaney, E. J.; Boppart, S. A.; Cheng, J. Non-Invasive, Real-Time Reporting Drug Release in Vitro and in Vivo. *Chem. Commun.* **2015**, *51* (32), 6948–6951. https://doi.org/10.1039/C4CC09920F.

(6) Kaupp, G.; Schmeyers, J.; Boy, J. Quantitative Solid-State Reactions of Amines with Carbonyl Compounds and Isothiocyanates. *Tetrahedron* **2000**, *56* (36), 6899–6911. https://doi.org/10.1016/S0040-4020(00)00511-1.

(7) Amemori, S.; Kokado, K.; Sada, K. Polymer Phase-Transition Behavior Driven by a Charge-Transfer Interaction. *Angew. Chem. Int. Ed.* **2013**, *52* (15), 4174–4178. https://doi.org/10.1002/anie.201210261.

(8) Sharma, A.; Kishore, D.; Singh, B. An Expedient Method for the Synthesis of 1,2,4-Triazolo-Fused 1,5-Benzodiazepine, 1,5-Benzoxazepine, and 1,5-Benzothiazepine Scaffolds: A Novel Seven-Membered Ring System of Biological Interest. *J. Heterocycl. Chem.* **2018**, *55* (3), 586–592. https://doi.org/10.1002/jhet.3060.

(9) Tuo, D.-H.; He, Q.; Wang, Q.-Q.; Ao, Y.-F.; Wang, D.-X. Benzene Triimides: Facile Synthesis and Self-Assembly Study. *Chin. J. Chem.* **2019**, *37* (7), 684–688. https://doi.org/10.1002/cjoc.201900146.

(10) Nicholson, R. S. Theory and Application of Cyclic Voltammetry for Measurement of Electrode Reaction Kinetics. *Anal. Chem.* **1965**, *37* (11), 1351–1355. https://doi.org/10.1021/ac60230a016.

(11) Milshtein, J. D.; Kaur, A. P.; Casselman, M. D.; Kowalski, J. A.; Modekrutti, S.; Zhang, P. L.; Harsha Attanayake, N.; Elliott, C. F.; Parkin, S. R.; Risko, C.; Brushett, F. R.; Odom, S. A. High Current Density, Long Duration Cycling of Soluble Organic Active Species for Non-Aqueous Redox Flow Batteries. *Energy Environ. Sci.* **2016**, *9* (11), 3531–3543. https://doi.org/10.1039/C6EE02027E.

(12) Cosimbescu, L.; Wei, X.; Vijayakumar, M.; Xu, W.; Helm, M. L.; Burton, S. D.; Sorensen, C. M.; Liu, J.; Sprenkle, V.; Wang, W. Anion-Tunable Properties and Electrochemical Performance of Functionalized Ferrocene Compounds. *Sci. Rep.* **2015**, *5* (1), 14117. https://doi.org/10.1038/srep14117.

(13) Wei, X.; Duan, W.; Huang, J.; Zhang, L.; Li, B.; Reed, D.; Xu, W.; Sprenkle, V.; Wang, W. A High-Current, Stable Nonaqueous Organic Redox Flow Battery. *ACS Energy Lett.* **2016**, *1* (4), 705–711. https://doi.org/10.1021/acsenergylett.6b00255.

(14) Duan, W.; Huang, J.; Kowalski, J. A.; Shkrob, I. A.; Vijayakumar, M.; Walter, E.; Pan, B.; Yang, Z.; Milshtein, J. D.; Li, B.; Liao, C.; Zhang, Z.; Wang, W.; Liu, J.; Moore, J. S.; Brushett, F. R.; Zhang, L.; Wei, X. "Wine-Dark Sea" in an Organic Flow Battery: Storing Negative Charge in 2,1,3-Benzothiadiazole Radicals Leads to Improved Cyclability. *ACS Energy Lett.* **2017**, *2* (5), 1156–1161. https://doi.org/10.1021/acsenergylett.7b00261.

(15) Zhang, C.; Niu, Z.; Ding, Y.; Zhang, L.; Zhou, Y.; Guo, X.; Zhang, X.; Zhao, Y.; Yu, G. Highly Concentrated Phthalimide-Based Anolytes for Organic Redox Flow Batteries with Enhanced Reversibility. *Chem* **2018**, *4* (12), 2814–2825. https://doi.org/10.1016/j.chempr.2018.08.024.

(16) Duan, W.; Vemuri, R. S.; Milshtein, J. D.; Laramie, S.; Dmello, R. D.; Huang, J.; Zhang, L.; Hu, D.; Vijayakumar, M.; Wang, W.; Liu, J.; Darling, R. M.; Thompson, L.; Smith, K.; Moore, J. S.; Brushett, F. R.; Wei, X. A Symmetric Organic-Based Nonaqueous Redox Flow Battery and Its State of Charge Diagnostics by FTIR. *J. Mater. Chem. A* **2016**, *4* (15), 5448–5456. https://doi.org/10.1039/C6TA01177B.

(17) Zhang, C.; Qian, Y.; Ding, Y.; Zhang, L.; Guo, X.; Zhao, Y.; Yu, G. Biredox Eutectic Electrolytes Derived from Organic Redox-Active Molecules: High-Energy Storage Systems. *Angew. Chem.* **2019**, *131* (21), 7119–7124. https://doi.org/10.1002/ange.201902433.

(18) Chen, H.; Niu, Z.; Ye, J.; Zhang, C.; Zhang, X.; Zhao, Y. Multicore Ferrocene Derivative as a Highly Soluble Cathode Material for Nonaqueous Redox Flow Batteries. *ACS Appl. Energy Mater.* **2021**, *4* (1), 855–861. https://doi.org/10.1021/acsaem.0c02733.

(19) Zhang, L.; Qian, Y.; Feng, R.; Ding, Y.; Zu, X.; Zhang, C.; Guo, X.; Wang, W.; Yu, G. Reversible Redox Chemistry in Azobenzene-Based Organic Molecules for High-Capacity and Long-Life Nonaqueous Redox Flow Batteries. *Nat. Commun.* **2020**, *11* (1), 3843. https://doi.org/10.1038/s41467-020-17662-y.

(20) Xing, X.; Liu, Q.; Xu, W.; Liang, W.; Liu, J.; Wang, B.; Lemmon, J. P. All-Liquid Electroactive Materials for High Energy Density Organic Flow Battery. *ACS Appl. Energy Mater.* **2019**, *2* (4), 2364–2369. https://doi.org/10.1021/acsaem.8b01874.

(21) Kwon, G.; Lee, K.; Lee, M. H.; Lee, B.; Lee, S.; Jung, S.-K.; Ku, K.; Kim, J.; Park, S. Y.; Kwon, J. E.; Kang, K. Bio-Inspired Molecular Redesign of a Multi-Redox Catholyte for High-Energy Non-Aqueous Organic Redox Flow Batteries. *Chem* **2019**, *5* (10), 2642–2656. https://doi.org/10.1016/j.chempr.2019.07.006.

(22) Hu, B.; Liu, T. L. Two Electron Utilization of Methyl Viologen Anolyte in Nonaqueous Organic Redox Flow Battery. *J. Energy Chem.* **2018**, *27* (5), 1326–1332. https://doi.org/10.1016/j.jechem.2018.02.014.